



Strong reconnection electric fields in shock-driven turbulence

Cite as: Phys. Plasmas **29**, 042304 (2022); <https://doi.org/10.1063/5.0077529>

Submitted: 03 November 2021 • Accepted: 23 March 2022 • Published Online: 08 April 2022

 N. Bessho, L.-J. Chen,  J. E. Stawarz, et al.

COLLECTIONS

Paper published as part of the special topic on [Plasma Physics from the Magnetospheric Multiscale Mission](#)



View Online



Export Citation



CrossMark

ARTICLES YOU MAY BE INTERESTED IN

[Turbulence-driven magnetic reconnection and the magnetic correlation length: Observations from Magnetospheric Multiscale in Earth's magnetosheath](#)

Phys. Plasmas **29**, 012302 (2022); <https://doi.org/10.1063/5.0071106>

[Theory, observations, and simulations of kinetic entropy in a magnetotail electron diffusion region](#)

Phys. Plasmas **29**, 022902 (2022); <https://doi.org/10.1063/5.0073248>

[Non-thermal electron velocity distribution functions due to 3D kinetic magnetic reconnection for solar coronal plasma conditions](#)

Phys. Plasmas **29**, 022104 (2022); <https://doi.org/10.1063/5.0061151>

Physics of Plasmas

Papers from 62nd Annual Meeting of the
APS Division of Plasma Physics

Read now!



Strong reconnection electric fields in shock-driven turbulence

Cite as: Phys. Plasmas **29**, 042304 (2022); doi: [10.1063/5.0077529](https://doi.org/10.1063/5.0077529)

Submitted: 3 November 2021 · Accepted: 23 March 2022 ·

Published Online: 8 April 2022



View Online



Export Citation



CrossMark

N. Bessho,^{1,2,a)}  L.-J. Chen,² J. E. Stawarz,³  S. Wang,^{1,2}  M. Hesse,⁴ L. B. Wilson III,²  and J. Ng^{1,2} 

AFFILIATIONS

¹Department of Astronomy, University of Maryland, College Park, Maryland 20742, USA

²Heliophysics Science Division, NASA Goddard Space Flight Center, Greenbelt, Maryland 20771, USA

³Department of Physics, Imperial College London, London SW7 2AZ, United Kingdom

⁴NASA Ames Research Center, Moffett Field, California 94035, USA

Note: This paper is a part of the Special Collection: Plasma Physics from the Magnetospheric Multiscale Mission.

a) Author to whom correspondence should be addressed: naoki.bessho@nasa.gov

ABSTRACT

Turbulent magnetic reconnection in a quasi-parallel shock under parameters relevant to the Earth's bow shock is investigated by means of a two-dimensional particle-in-cell simulation. The addressed aspects include the reconnection electric field, the reconnection rate, and the electron and the ion outflow speeds. In the shock transition region, many current sheets are generated in shock-driven turbulence, and electron-only reconnection and reconnection where both ions and electrons are involved can occur in those current sheets. The electron outflow speed in electron-only reconnection shows a positive correlation with the theoretical speed, which is close to the local electron Alfvén speed, and a strong convection electric field is generated by the large electron outflow. As a result, the reconnection electric field becomes much larger than those in the standard magnetopause or magnetotail reconnection. In shock-driven reconnection that involves ion dynamics, both electron outflows and ion outflows can reach of the order of 10 times the Alfvén speed in the X-line rest frame, leading to a reconnection electric field the same order as that in electron-only reconnection. An electron-only reconnection event observed by the magnetospheric multiscale mission downstream of a quasi-parallel shock is qualitatively similar to those in the simulation and shows that the outflow speed reaches approximately half the local electron Alfvén speed, supporting the simulation prediction.

© 2022 Author(s). All article content, except where otherwise noted, is licensed under a Creative Commons Attribution (CC BY) license (<http://creativecommons.org/licenses/by/4.0/>). <https://doi.org/10.1063/5.0077529>

I. INTRODUCTION

Electron-only reconnection is a new type of magnetic reconnection that has been gathering attention recently. In such reconnection, only electrons show outflow jets, and no ion jets are generated. Electron-only reconnection was first detected by NASA's Magnetospheric Multiscale (MMS) mission in the Earth's magnetosheath,¹ where a large number of current sheets are generated due to the shock turbulence in the downstream region of a quasi-parallel bow shock. Since the size of these current sheets is much smaller than ion gyro-radii, ions cannot respond to the sudden change of magnetic fields in those current sheets, and only electrons participate in magnetic reconnection. As a result, electron jets are generated, but ions are just passing through those regions without generating jets.

Later, MMS observed electron-only reconnection in the shock transition region,^{2–5} the magnetosheath,^{6,7} and the foreshock region^{8,9} of the Earth's bow shock. In addition, possible signatures of

electron-only reconnection were found in the magnetic spectrum in turbulence in the magnetosheath.¹¹ On the other hand, electron-only reconnection was also observed in the Earth's magnetotail,¹⁰ and it is interpreted to be the early stage of regular reconnection. In the early stage, the size of the diffusion region is small and only electron jets are generated. The ion jets are generated in the subsequent stage after the electron jets grow, and regular reconnection proceeds with both ions and electrons.

Electron-only reconnection has been studied by numerical simulations as well, by means of particle-in-cell (PIC) simulations^{12–16} and hybrid Vlasov–Maxwell simulations.^{17,18} In our previous studies by two-dimensional (2D) PIC simulations, to understand the physics of electron-only reconnection, we investigated quasi-parallel shocks whose shock normal angle is 25°. ^{13,14} In those studies, we demonstrated that when the Alfvén Mach number ($M_A = v_{sh}/v_{A0}$, where v_{sh} is the shock speed, and v_{A0} is the upstream Alfvén speed) is around 10

and when the shock speed is smaller than the electron thermal speed, many current sheets with their thicknesses a few ion skin depths are generated in the shock transition region due to the ion–ion nonresonant beam instability, and the subsequent secondary instability generates many sub-ion-scale modulations in magnetic fields and current sheets with their thicknesses several electron skin depths, in which electron-only reconnection can occur. In electron-only reconnection, electron distribution functions show that the temperature is higher than the upstream region, and electrons are accelerated in the direction opposite to the reconnection electric field. Due to the acceleration, the electron outflow speed almost reaches the electron Alfvén speed.

In contrast, regular reconnection, where both ions and electrons are involved, also occurs in shocks, and both species can be accelerated. In the same shock simulation with the 25° shock angle, one of the regions of regular reconnection, where the ion–ion nonresonant beam instability generates ion-scale modulations in magnetic fields, was investigated, and we observed that both ion and electron jets are generated.

In this study, we analyze the properties of reconnection electric fields in electron-only reconnection and regular reconnection in the Earth’s quasi-parallel bow shock, using a 2D PIC simulation. We will statistically investigate outflow speeds in both electron-only reconnection and regular reconnection, and the magnitude of the reconnection electric field and reconnection rates. Section II explains the simulation method. In Sec. III, we investigate reconnection in the shock transition region and discuss the analysis results. In Sec. IV, we show an example of observation by MMS for electron-only reconnection. Section V summarizes this study.

II. SIMULATION METHOD

We perform a two-and-a-half dimensional electromagnetic PIC simulation for a quasi-parallel shock, where the simulation domain is in 2D, but three vector components in field quantities and particle velocities are treated. The details of the simulation method are explained in the previous papers.^{13,14} The mass ratio of the ion to the electron is $m_i/m_e = 200$. The densities of both ions and electrons are uniform, and they are $n = n_0$ (100 particles per cell for each species) at the initial time $t = 0$. The magnetic field is also uniform at $t = 0$, and $\mathbf{B}_0 = [B_0 \cos \theta, B_0 \sin \theta, 0]$, where θ is the shock normal angle, and we use $\theta = 25^\circ$. The simulation domain has a size $L_x \times L_y = 375d_i \times 51.2d_i$, where d_i is the ion skin depth based on the initial density n_0 [$d_i = c/(4\pi n_0 e^2/m_i)^{1/2}$, where e is the elementary charge, and c is the light speed]. The ratio of the plasma frequency [$\omega_{pe} = (4\pi n_0 e^2/m_e)^{1/2}$] to the electron cyclotron frequency ($\Omega_e = eB_0/m_e c$) is $\omega_{pe}/\Omega_e = 4.0$, which gives $v_{A0}/c = 1/56.6$, where v_{A0} is the Alfvén speed based on B_0 and n_0 . The beta values at $t = 0$ for the ions and the electrons are $\beta_i = 1.0$ and $\beta_e = 1.0$, respectively. With these parameters, the electron thermal speed becomes $v_{Te} = 14.1v_{A0}$. Conducting walls are placed at $x = 0$ and $x = L_x$, where particles are specularly reflected, while we use periodic boundaries in the y direction.

To drive a shock wave, we impose a uniform electric field E_z and give a negative x speed $v_d = -9.0v_{A0}$ to all the particles, where $E_z = -v_d B_0 \sin \theta / c$. The conducting wall at $x = 0$ reflects all the particles, which generates strong disturbances in the magnetic field, and eventually, a shock wave is generated, propagating in the x direction with a positive speed. Since all the particles are drifting to the negative x direction throughout the simulation time, we inject new particles

from the boundary at $x = L_x$. The shock speed v_{sh} is determined by the speed of the largest magnetic pulse in the x direction, adding the drift speed $|v_d|$.

III. OUTFLOW SPEEDS AND RECONNECTION ELECTRIC FIELDS IN THE SHOCK TRANSITION REGION

A. Categorization of reconnection X lines

We investigate reconnecting current sheets generated in the shock transition region. The details of several reconnecting current sheets in the shock transition region in the same simulation have already been documented in the previous papers.^{13,14} In this paper, our focus is the outflow speed and the reconnection electric field, which is the magnitude of E_z field at the X line in each reconnection region.

Figure 1(a) shows the current density J_z and magnetic field lines in a simulation domain, $40 < x/d_i < 55$ and the whole y range $0 < y/d_i < 51.2$, at $\Omega_i t = 18.75$, where Ω_i is the ion cyclotron frequency based on B_0 . The gray lines are magnetic field lines, which are the contour of the vector potential A_z , and the color contour shows J_z . The plotted region is the shock transition region. The right side ($55d_i < x$) is the upstream region, while the left side ($x < 40d_i$) is the downstream region. The Alfvén Mach number ($M_A = v_{sh}/v_{A0}$) is 11.4, and the magnetic field strength becomes almost six times larger in the shock than the upstream value. For details of the shock evolution, please refer to the previous studies.^{13,14} Those current sheets are generated due to two types of instabilities: a nonresonant ion–ion beam instability (in which the fastest growing mode does not resonate with the reflected ions but with the incoming solar wind), and the secondary instability due to multiple electron and ion beams.

In the right panel (b), the positions of X lines are marked by Xs. We identified 43 X lines in this region and traced the motion of these 43 X lines for 100 time steps from $\Omega_i t = 18.75$ –18.78. In these 43 X lines, we only analyze 32 X lines that are stable during the time interval. The rest 11 X-line regions have one or multiple magnetic islands disappeared within the 100 time steps, which is difficult to analyze, and hence, they are not included. Figure 1(b) shows these 32 X lines.

For these 32 X lines, we determine whether there exist electron jets in each reconnection region. When no electron jets are confirmed around an X line, we categorize the region as “no active reconnection,” which indicates that either reconnection has already ceased, or reconnection has just begun and no jet has been developed yet. For the X lines where electron jets are observed, we investigate whether there are ion jets. When no ion jet is observed around an X line with electron jets, we categorize the X line as “electron-only reconnection.” In X lines where ion jets are confirmed, there are some X lines where the electron jet points to a direction different from the ion jet. For example, there is an X line where the electron jet and the ion jet are almost counterstreaming. Since there is a shock turbulence, strong ion flows can be generated without reconnection, and such strong ion flows can pass through a small-scale electron-only reconnection region. Therefore, we categorize those X lines as “electron-only reconnection,” because electron and ion jet motions are decoupled. When an X line shows both electron and ion jets pointing in the same direction (the angle between the electron and ion jets less than 10°) or similar directions (the angle $\leq 45^\circ$) from the X line, and when the ion speed increases from the X line to the downstream region, we categorize the X line as “regular reconnection.” In Fig. 1(b), magenta Xs show the

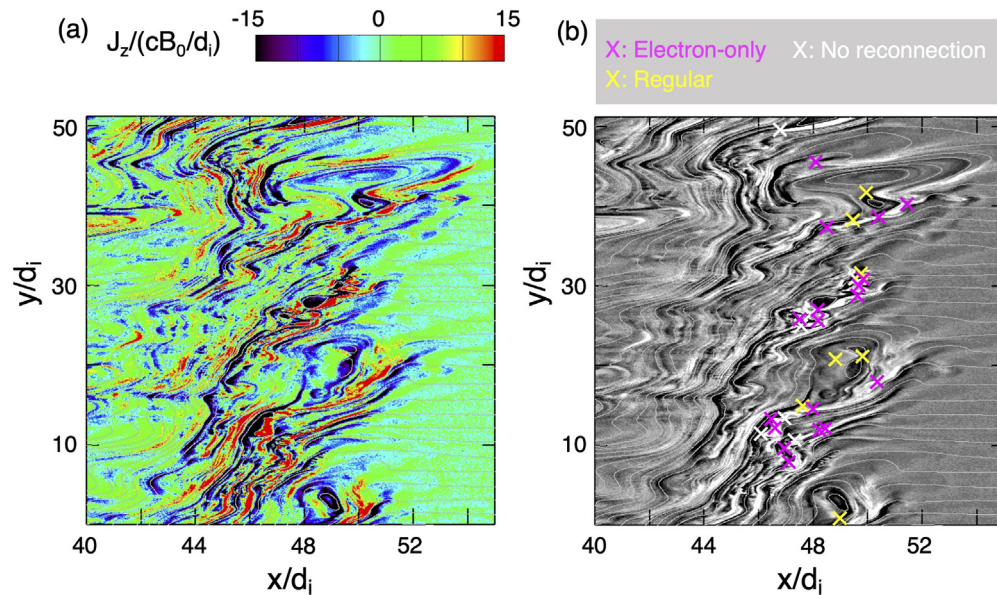


FIG. 1. (a) Current density J_z in the shock transition region. Gray curves are magnetic field lines projected on the x - y plane. (b) Positions of electron-only reconnection (magenta Xs), regular reconnection (yellow Xs), and no active reconnection (white Xs).

positions of electron-only reconnection, yellow Xs show the positions of regular reconnection, and white Xs mark the positions of no active reconnection. In these 32 X lines, 18 X lines show electron-only reconnection, 7 X lines show regular reconnection, and 7 X lines show no active reconnection.

In the shock-driven turbulence, the shape of each reconnection region is significantly distorted, and most reconnection shows asymmetry in both the inflow direction and the outflow direction. As a result, many reconnection regions show only a one-sided jet, which points in a certain direction without the counterpart of the jet pointing in the opposite direction. Later in Sec. III D, we will discuss asymmetry in the outflow direction in such a reconnection site with a one-sided jet. In the 18 sites of electron-only reconnection, nine reconnection sites show only one-sided jets, and the rest nine sites show two-sided jets. In the seven regular reconnection sites, only one site shows both two-sided electron jets and two-sided ion jets. There are three sites that show two-sided electron jets and one-sided ion jets. The rest three sites show one-sided electron jets and one-sided ion jets.

Comparing Figs. 1(a) and 1(b), we notice that regular reconnection (yellow Xs) occurs where there are large-scale magnetic islands. For example, there is a large-scale island (whose size is a few d_i) around $x = 50d_i$ and $y = 42d_i$, and there are two yellow X lines at $(x, y) = (49.45d_i, 38.275d_i)$ and $(49.925d_i, 41.825d_i)$. Another one is found near a large-scale island around $x = 49d_i$ and $y = 2d_i$, and there is a regular reconnection site whose X line is at $(x, y) = (48.975d_i, 0.925d_i)$. This is because regular reconnection is often associated with the nonresonant ion-ion beam instability, which generates a magnetic field modulation whose size is of the order of d_i . Magnetic field lines bend more and more as the waves grow, and eventually reconnection occurs when the bent field lines generate a loop-like structure where two oppositely directed field lines are in contact at a point. If reconnection occurs due to this instability, regular

reconnection is realized because ions can respond to such a large-scale (ion-scale) structure. The positions of yellow Xs in Fig. 1(b) are seen near large-scale magnetic flux ropes (magnetic islands). In contrast, electron-only reconnection sites (magenta Xs) are distributed in regions with fine-scale current structures. For example, in the region around $x = 50d_i$ and $y = 30d_i$, there are fine structures of current sheets [intricate patterns of red and black regions; see panel (a)], where several magenta Xs are seen. Another region with turbulent current sheets is seen near $x = 47d_i$ and $y = 10d_i$, and there are many magenta Xs. These regions are where the secondary instability occurs after the nonresonant ion-ion beam instability, and many small-scale (sub- d_i scale) current sheets are generated. Please refer to Ref. 14 for more details about the instabilities in the shock. In these regions, since ions cannot respond quickly to such small-scale changes of magnetic fields, electron-only reconnection can occur.

B. Electron-only reconnection

Figure 2 shows an example of a reconnecting current sheet where electron-only reconnection occurs. The plots are as follows: (a) the current density J_z , (b) the out-of-plane electric field E_z , (c) the in-plane electron fluid velocity $V_e = (V_{ex}^2 + V_{ey}^2)^{1/2}$ multiplied by the sign of V_{ey} , (d) the in-plane ion fluid velocity $V_i = (V_{ix}^2 + V_{iy}^2)^{1/2}$ multiplied by the sign of V_{iy} , (e) the out-of-plane magnetic field B_z , and (f) one-dimensional (1D) plots of the magnetic field B_L and the electron density n_e across the current sheet. For the in-plane electric field E_x and E_y , please see the [supplementary material](#). The coordinates L and N are shown in panel (d). These quantities are in the X-line rest frame, where the X-line position is stationary. To obtain the X-line rest frame, we measured the velocity of the X-line motion in the simulation (for 100 time steps from $\Omega_i t = 18.75$ – 18.78 , measuring the position at every 10 time step), and we changed the frame from the original

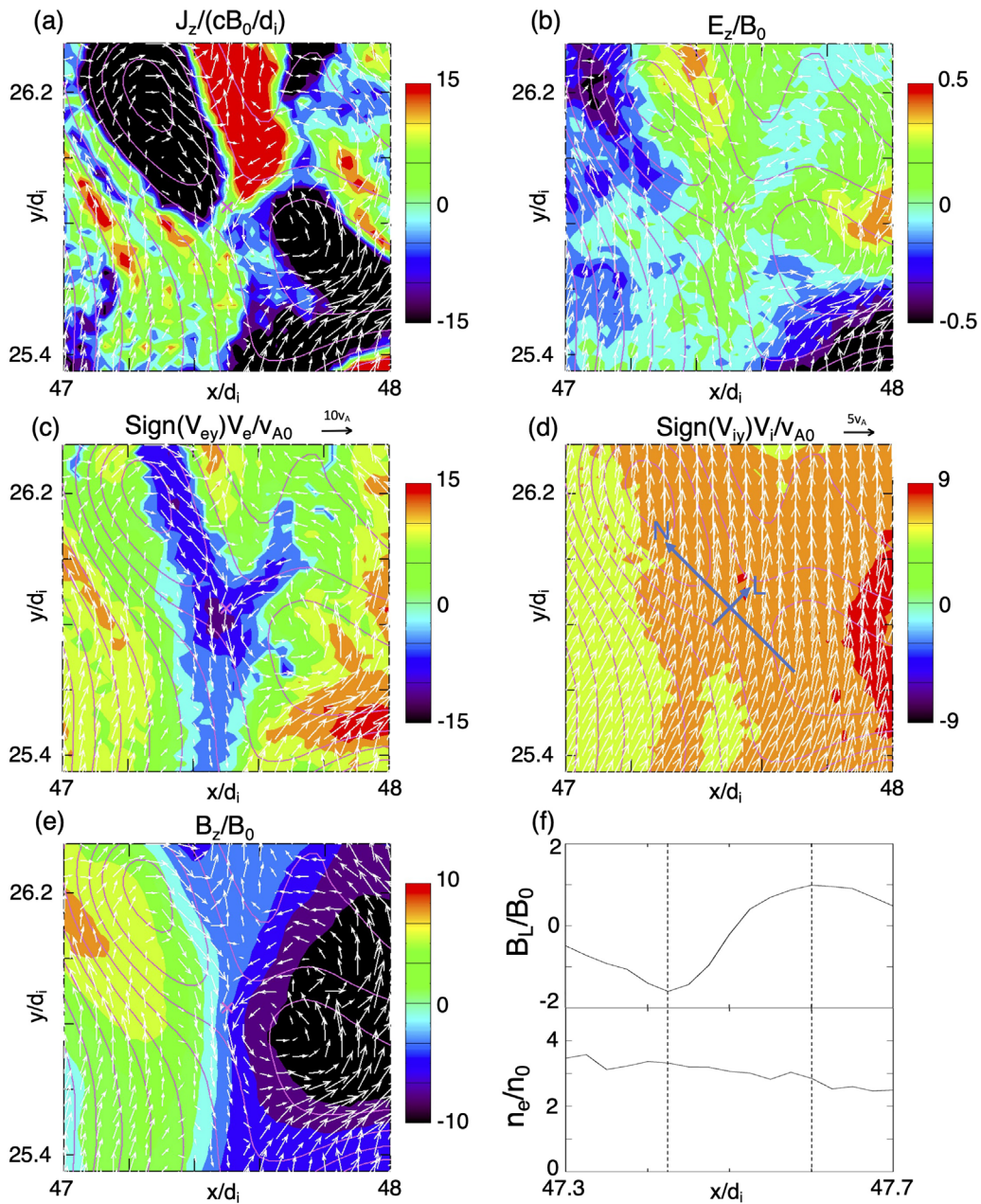


FIG. 2. Field quantities in an electron-only reconnection site, in the X-line rest frame. The X line is at $(x, y) = (47.5d_i, 25.85d_i)$, indicated by the magenta X in each plot. (a) Current density J_z , (b) electric field E_z , (c) the in-plane electron fluid velocity $V_e = (V_{ex}^2 + V_{ey}^2)^{1/2}$ multiplied by $\text{sign}(V_{ey})$, (d) the in-plane ion fluid velocity V_i multiplied by $\text{sign}(V_{iy})$, (e) magnetic field B_z , and (f) 1D cuts of B_L and the electron density n_e along the N direction. L is the direction of the reconnecting magnetic field B_L , and L - N coordinates are shown in panel (d). The cuts are along the N axis. In all the plots, magenta curves are magnetic field lines. White arrows in panels (a)–(c) and (e) are the electron fluid velocity vectors in the X-line rest frame, while those in panel (d) are the ion fluid velocity vectors. The two vertical dashed lines in panel (f) indicate the positions where we measured $B_1, B_2, n_1,$ and n_2 for the asymmetric reconnection theory.

simulation frame to the X-line rest frame. Suppose the X-line speed is V_X , we have $E_{z,rest} = E_{z,sim} + (\mathbf{V}_X \times \mathbf{B})_z/c$, where $E_{z,rest}$ and $E_{z,sim}$ are the electric field E_z in the X-line rest frame and in the simulation frame, respectively. In each panel, white arrows represent the vectors

of the electron fluid velocity, except for the ion fluid velocity plot [panel (d)], where the white arrows are the vectors of the ion fluid velocity. The X line is shown by the magenta X, and magenta lines are magnetic field lines.

In these panels, the X line is located at $(x, y) = (x_X, y_X) = (47.5d_i, 25.85d_i)$. The current density J_z [panel (a)] shows a diagonally negative (black) structure from the top left quadrant ($x < x_X$ and $y < y_X$) to the bottom right quadrant ($x < x_X$ and $y > y_X$) around the X line, and this negative J_z is separated by the positive current sheet (green and red) around the X line, which shows also a diagonal structure passing from the top right quadrant ($x > x_X$ and $y < y_X$) to the bottom left quadrant ($x > x_X$ and $y > y_X$) around the X line. Because of this positive current sheet, two magnetic islands are seen in the top left and the bottom right regions. Regarding the magnetic field direction, if we use the L - N coordinates [see panel (d)], where L is the direction of the reconnecting magnetic field, $B_L < 0$ in the upper region (above the positive current sheet), and $B_L > 0$ in the lower region (below the positive current sheet).

Panel (c) for V_e shows an electron jet that passes through the X line almost vertically from top to bottom. The maximum of the in-plane electron outflow speed $(V_{ex}^2 + V_{ey}^2)^{1/2}$ in the X-line rest frame is $V_{out} = 10.7v_{A0}$ at $(x, y) = (47.5d_i, 25.8d_i)$, slightly below the X line. Let us apply the reconnection model by Ref. 20 for asymmetric reconnection to discuss the outflow speed. The magnetic field strengths at the two sides across the current sheet in the N direction [see panel (f)] are $B_1 = 1.6B_0$ and $B_2 = 0.99B_0$, and the electron densities at the two sides are $n_1 = 3.3n_0$ and $n_2 = 2.9n_0$. Here, to compute B_1 and B_2 , we first visually determined the current sheet normal direction N as in panel (d), and then investigate the L component of the magnetic field, which is perpendicular to the N direction, along the N direction passing through the X line to find the two maxima positions of $|B_L|$, as shown in panel (f). We assume that these two maxima of $|B_L|$ represent B_1 and B_2 , and also measured the densities n_1 and n_2 at the two positions. Using the asymmetric reconnection model, the outflow speed is predicted to be $V_{theory} = [B_1B_2(B_1 + B_2)/(n_1B_2 + n_2B_1)]^{1/2} (1/4\pi m_e)^{1/2} = 10.2v_{A0}$, which is consistent with the observed electron outflow $10.7v_{A0}$. Note that this theoretical speed V_{theory} is close to the local electron Alfvén speed. For example, at the position with B_1 and n_1 , the local electron Alfvén speed is $12.4v_{A0}$, while at the position with B_2 and n_2 , the local electron Alfvén speed is $8.3v_{A0}$. Therefore, the electron outflow speed is close to those local electron Alfvén speeds. In contrast, the ion fluid velocity [panel (d)] shows no ion jet, and this reconnection is only due to electrons. As shown in panel (c), this electron-only reconnection has a one-sided jet. We will discuss later the applicability of the asymmetric reconnection theory to reconnection in a shock, considering both one-sided and two-sided jets (see Subsection III D). Also, more details about the flow patterns in this reconnection region and the size of the electron diffusion region (EDR) are shown in Fig. S1 in the supplementary material.

The electric field E_z in the X-line rest frame [panel (b)] shows a positive value around the X line, which is due to the electron flow pointing in the negative y direction. Note that the convection electric field $E_z = -(V_{ex}B_y - V_{ey}B_x)/c \sim V_{ey}B_x/c$ with $V_{ey} < 0$ and $B_x < 0$ below the X line. The reconnection electric field E_r ($|E_z|$ at the X line) is $E_r = 0.075B_0$. The reconnection rate $R = E_r/(B_d V_{theory}/c)$, where $B_d = 2B_1B_2/(B_1 + B_2)$, is 0.34, and R based on the outflow speed V_{out} instead of V_{theory} is 0.32.

Note that there are strong electron inflows from three directions [see panel (c) in Fig. 2 and panel (a) in Fig. S1 in the supplementary material]: There are two inflows in the N direction, and the other is from the positive L side (flow along the positive current sheet). Two of

these inflows (the one from the positive y direction toward the X line, and the one in the L direction toward the X line) show large speeds around $8v_{A0}$, and each of these inflows also generates a large convection electric field E_z . The inflow from the positive y side generates a positive E_z due to $V_{ey}B_x/c$ with $V_{ey} < 0$ and $B_x < 0$, but the other inflow from the positive L side generates a negative convection electric field (not shown) $E_z \sim -V_{eL}B_N/c$ with $V_{eL} < 0$ and $B_N < 0$. This unusual L -directional inflow is not seen in the standard laminar reconnection, but this is generated in the shock-turbulent reconnection. However, due to the demagnetization of the electron in the diffusion region (see Fig. S1 in the supplementary material), the effect of the nonideal electric field surpasses the convection electric field, and the reconnection region shows a positive E_z near the X line. This reconnection is driven by these strong inflows, similar to reconnection driven by a Kelvin–Helmholtz instability.¹⁹

Panel (e) shows that there exists a large-amplitude B_z , out of plane with respect to the reconnection plane N - L . At the X line, $B_z = -3B_0 = -2.5B_d$, and this reconnection involves a strong guide field.

Figure 3 shows another example of a reconnecting current sheet. The current density J_z [panel (a)] shows an almost vertical negative current sheet at the X line, $(x, y) = (x_X, y_X) = (48.5d_i, 37.375d_i)$. Magnetic fields point upward ($B_y > 0$) in the region left to the X line ($x < x_X$), while they point downward ($B_y < 0$) in the region right to the X line ($x > x_X$). The electron velocity V_e [panel (c)] shows an almost vertical downward jet ($V_{ex} < 0$ and $V_{ey} < 0$) in the left bottom quadrant ($x < x_X$ and $y < y_X$) from the X line, and the maximum speed is $5.0v_{A0}$ at $(x, y) = (48.3d_i, 36.95d_i)$. The details about the flow patterns and the size of the EDR are shown in Fig. S2 in the supplementary material.

Even though the negative current sheet across the X line forms almost along the y direction, the B_x component (instead of B_y component) is the reconnecting magnetic field. We decided the direction of the reconnection (which side is the inflow and which side is the outflow) based on the time evolution of the vector potential A_z . According to the evolution of A_z (not shown), we found that the magnetic island in the positive y side becomes smaller as time elapses, and this means that the direction of the B_L component (reconnecting magnetic field) is in the x direction. Panel (d) shows the N and L directions around the X line, and $B_L < 0$ above the X line, while $B_L > 0$ below the X line. The ion velocity V_i does not show an ion jet, and this is electron-only reconnection. Using the asymmetric reconnection model [$B_1 = 0.44B_0$, $B_2 = 0.36B_0$, $n_1 = 3.5n_0$, and $n_2 = 3.3n_0$; see panel (f)], the outflow speed is predicted to be $V_{theory} = 3.1v_{A0}$, which is close to the observed electron outflow $V_{out} = 5.0v_{A0}$.

The electric field E_z [panel (b)] is positive around the X line, and the reconnection electric field is $E_r = 0.005B_0$. This means that the sign of the reconnection electric field is opposite to the sign of the current density J_z , which resembles reconnection with a current sheet with the opposite sign to the reconnection electric field in Ref. 21. In our case, this condition results in a negative energy exchange rate [i.e., $\mathbf{J} \cdot (\mathbf{E} + \mathbf{V}_e \times \mathbf{B}/c) < 0$] at the X line; however, there exist positive regions of the energy exchange rate near the X line [see panel (e) in Fig. S2 in the supplementary material], slightly offset from the X line (near the negative E_z region in the vicinity of the X line, as well as part of the outflow region near the outflow maximum), and the overall energy exchange rate in the reconnection region is positive. Using the

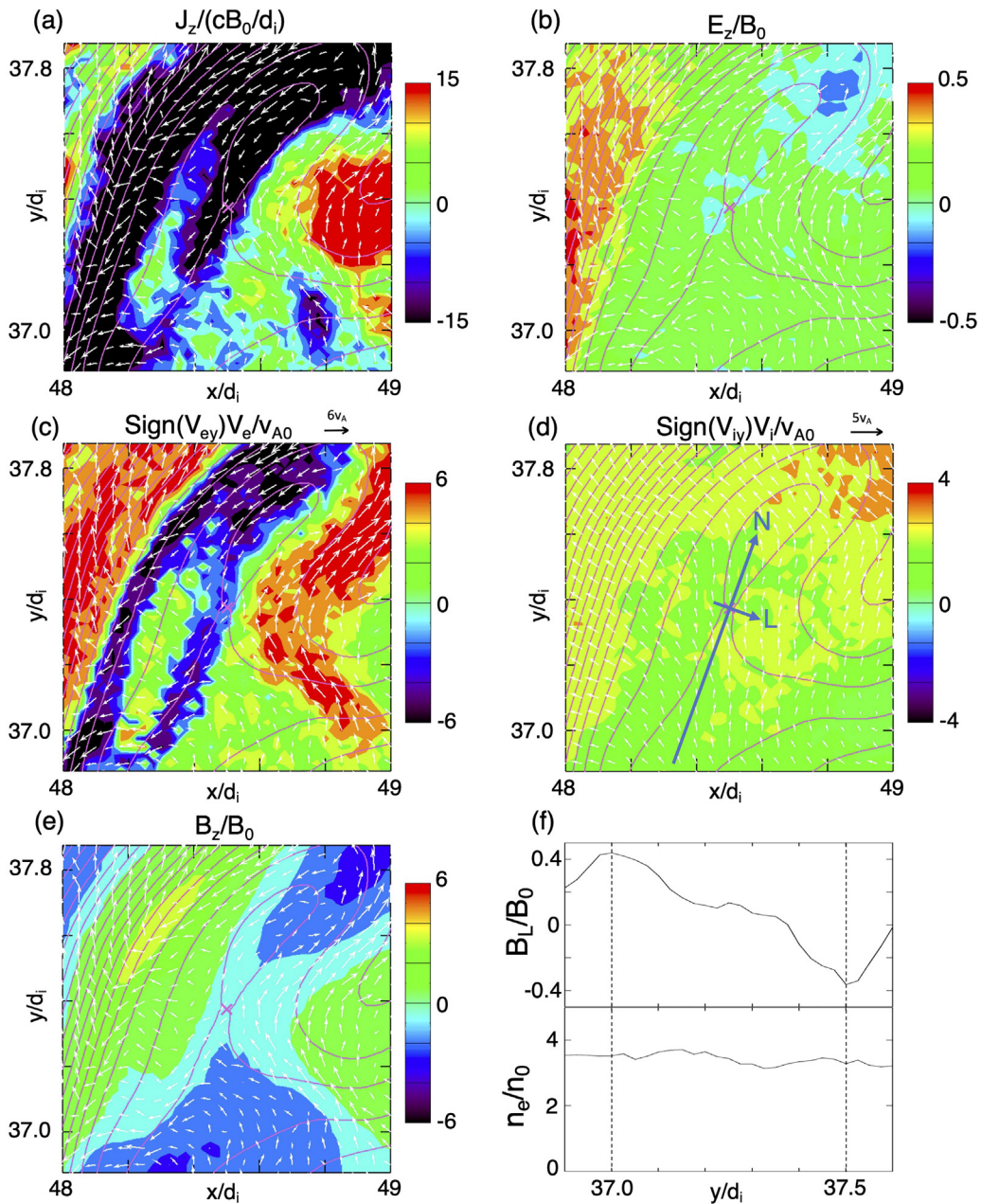


FIG. 3. Field quantities in another electron-only reconnection site in the X-line rest frame, at the X line $(x, y) = (48.5d_i, 37.375d_i)$, in the same format as in Fig. 2.

asymmetric reconnection model, the reconnection rate is $R = E_r / (B_d V_{theory} / c) = 0.24$, and if we use V_{out} , $R = 0.14$. Panel (e) shows that the guide field strength at the X line is $B_z = -0.69B_0 = -1.7B_d$.

In these electron-only reconnection sites, most of the electron outflow speeds are of the order of electron Alfvén speed, and also close to the theoretical speed defined in the asymmetric reconnection theory, that is, V_{theory} . The reconnection electric fields E_r in these sites are of the order of $0.1 B_d V_{theory} / c$; that is, the reconnection rate $[R = E_r / (B_d V_{theory} / c)]$ is of the order of 0.1. Compared with the

reconnection rate of standard reconnection in the Earth's magnetopause/magnetotail,^{22–25} where both ions and electrons are responsible for reconnection, the reconnection rate is the same order, around 0.1; however, the reconnection rate of 0.1 in electron-only reconnection indicates that the reconnection electric field is unusually larger than the reconnection electric field in the standard reconnection in the magnetopause/magnetotail. This is because the outflow velocity V_{out} which is close to V_{theory} in electron-only reconnection is of the order of the electron Alfvén speed v_{Ae} . Therefore, the reconnection electric

field in electron-only reconnection is of the order of $0.1 B_d v_{Ae}/c = 0.1(m_i/m_e)^{1/2} B_d v_A/c$, which is $(m_i/m_e)^{1/2}$ larger than the reconnection electric field in the standard laminar reconnection in the Earth's magnetopause/magnetotail, $0.1 B_d v_A/c$. Our argument is consistent with Ref. 12, in which the reconnection electric field is compared between electron-only reconnection and the standard reconnection. More discussions about the reconnection rates in both types of reconnection are given in Sec. III D.

To investigate the strength of the reconnection electric field E_r , we performed a statistical analysis for electron-only reconnection, even though the sample size is small. The following properties are investigated: (1) the reconnection electric field E_r ($|E_z|$ at the X line), (2) the reconnection rate [we consider two rates: $R_t = E_r/(B_d V_{theory}/c)$ and $R_o = E_r/(B_d V_{out}/c)$], and (3) the outflow speed

V_{out} . In the observed 18 electron-only reconnection X lines, three X lines show E_z with its sign opposite from what we expect by the evolution of the magnetic field lines (in other words, the evolution of the vector potential A_z). For example, the X line at $(x, y) = (51.425d_i, 40.3d_i)$ shows a negative E_z , but based on the time evolution of the magnetic field lines, the reconnection electric field should have a positive E_z . This discrepancy in the observed E_z may be due to the temporal variation in the reconnection electric field affected by the surrounding region, which is beyond the scope of this paper. We discard those three X lines that show E_z inconsistent with what we expect, and we use the rest 15 X lines for the statistical analysis.

Figure 4 shows histograms for the reconnection electric field E_r , the reconnection rates [$R_t = E_r/(B_d V_{theory}/c)$ and $R_o = E_r/(B_d V_{out}/c)$], and the electron outflow speed V_{out} . Figure 4(a) shows a

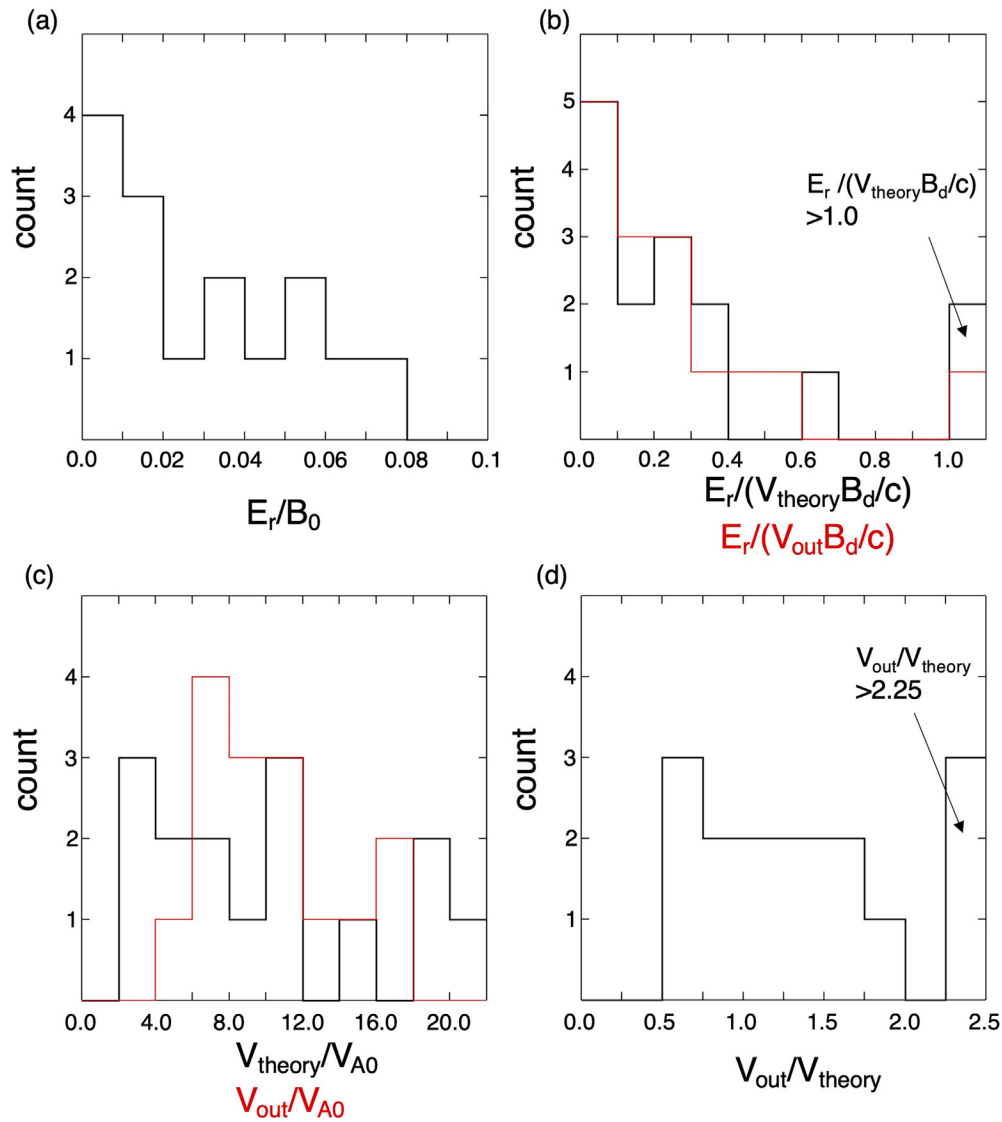


FIG. 4. Histograms for electron-only reconnection. (a) Reconnection electric field E_r , (b) reconnection rates $R_t = E_r/(V_{theory} B_d/c)$ (black) and $R_o = E_r/(V_{out} B_d/c)$ (red), (c) theoretical outflow speed V_{theory} (black) and observed outflow speed V_{out} (red), and (d) the ratio V_{out}/V_{theory} .

histogram for E_r normalized by the magnetic field B_0 in the shock upstream region. In the 15 X lines we analyzed, seven X lines have E_r less than 0.02, and the rest of the X lines range from 0.02 to 0.08. The mean is $0.031B_0$ ($= 0.36B_0 \sin \theta V_{sw}/c$, where $V_{sw} = 11.4v_{A0}$ represents the solar wind speed), the minimum is $0.0038B_0$ ($= 0.044B_0 \sin \theta V_{sw}/c$), and the maximum is $0.075B_0$ ($= 0.88B_0 \sin \theta V_{sw}/c$). Figure 4(b) shows two histograms: One is for the reconnection rate $R_t = E_r/(V_{theory}B_d/c)$ (black), and the other is for the reconnection rate $R_o = E_r/(V_{out}B_d/c)$ (red). In these 15 X lines, 12 X lines show R_t less than 0.4, and the rest three X lines show the reconnection rate R_t larger than 0.6. The two X lines indicated by the black arrow are the ones with $R_t > 1.0$ ($R_t = 1.4$ and 2.6). Including these three large reconnection rates, the mean is 0.43, but if we exclude these three as outliers, the mean of the 12 reconnection rates R_t is 0.16. In the total 15 reconnection rates, the minimum is 0.019, and the maximum is 2.6. For the reconnection rate R_o (red), where V_{out} is used, only one reconnection rate R_o shows larger than 1, and 14 reconnection rates are less than 0.6. The mean is 0.25, the minimum is 0.029, and the maximum is 1.0. Note that in the standard laminar reconnection, a theoretical study²⁶ shows that the upper limit of the reconnection rate should be smaller than around 0.5 in nonrelativistic cases. However, reconnection in the present study is driven reconnection due to strong flows in the shock turbulence, and in that case, reconnection rates can be much larger than 0.5.

Figures 4(c) and 4(d) show histograms for the outflow speed, V_{out} . Panel (c) shows histograms for V_{out} (red) and V_{theory} (black), normalized by the Alfvén speed in the upstream region v_{A0} [note that the electron Alfvén speed in the upstream is $v_{Ae0} = (m_i/m_e)^{1/2}v_{A0} = 14.1v_{A0}$ in the simulation with $m_i/m_e = 200$]. For the observed outflow speeds V_{out} (red), the speeds are distributed between $4.0v_{A0}$ and $18.0v_{A0}$, and the mean is $10.1v_{A0}$, which is 0.72 of the electron Alfvén speed $v_{Ae0} = 14.1v_{A0}$ in the upstream region. The minimum is $5.0v_{A0}$, and the maximum is $17.4v_{A0}$. However, the minimum value $5.0v_{A0}$ does not mean that the outflow speed at that reconnection site reaches much less than the local electron Alfvén speed, because the local electron Alfvén speed is close to V_{theory} . The black histogram is for V_{theory} and the values are spread between $2v_{A0}$ and $22v_{A0}$. Panel (d) shows a histogram for V_{out} normalized by the theoretical prediction speed, V_{theory} . Most of the X lines show V_{out}/V_{theory} around 1.0 (between 0.5 and 2.0). The minimum value of the outflow speed in panel (c), $V_{out} = 5.0v_{A0}$, corresponds to $V_{out}/V_{theory} = 1.6$; therefore, that outflow speed actually exceeds the predicted speed. The minimum of V_{out}/V_{theory} is 0.52, and the maximum is 3.4. Three X lines show larger than 2.25 ($V_{out}/V_{theory} = 2.4, 2.5,$ and 3.4). Therefore, all the electron outflows show larger than 0.5 of the predicted speed.

Figure 5 shows scatterplots for the outflow speed V_{out} , the reconnection electric field E_r , and the reconnection rates R_t and R_o . Panel (a) shows a plot for V_{out} as a function of V_{theory} . The outflow speeds V_{out} range from $5.0v_{A0}$ to $17.4v_{A0}$, and there is a positive correlation between V_{out} and the theoretical prediction V_{theory} . We investigated the correlation based on Spearman's rank correlation, since the sample size 15 is small, and the distributions of both V_{out} and V_{theory} are not Gaussian [see the histograms in Fig. 4(c)]. The Spearman's rank correlation coefficient is 0.75, and the p-value (using the t -distribution for the degrees of freedom $n - 2$, where n is the sample size) is 0.0013, which is less than 0.05 (5% significant level). We conclude that there is a strong positive correlation between V_{out} and V_{theory} , and the reconnection outflow V_{out} is well explained by the asymmetric reconnection

theory with using the electron mass m_e . Note that we confirmed that these reconnection regions show converging inflows in the N direction toward the X line (see examples in the [supplementary material](#)), which are necessary for reconnection [see also Eqs. (A2) and (A3) in the [Appendix](#) and Eq. (3) in Sec. III D]. As it is explained later in Sec. III D, the outflow speed V_{out} becomes close to V_{theory} , even under a strong background flow, as long as there exist converging inflows toward the X line. Therefore, the correlation between V_{out} and V_{theory} indicates that the outflows result from reconnection driven by the background flows.

Panel (b) shows the reconnection electric field E_r as functions of the theoretical speed V_{theory} (black) and the observed outflow speed V_{out} (red). Seeing the black scatterplot, it is hard to see a correlation between E_r and V_{theory} . In contrast, if we use the observed outflow speed V_{out} (red scatterplot), we can see a weak correlation between E_r and V_{out} . Since the distribution of E_r is also not a Gaussian [Fig. 4(a)], we performed Spearman's rank correlation analysis. The rank correlation coefficient is 0.33 for the red data points. However, the p-value is 0.23. This large p-value is mainly due to the small sample size, and we cannot conclude, with this p-value, whether there is a weak correlation. Nevertheless, we can at least say that there may be a tendency that the larger the outflow speed, the larger the reconnection electric field. To prove this, we need to increase the sample size. In the following analysis for other variables, if we find that the rank correlation coefficient is large but the p-value > 0.05 , we will interpret that there is a "tendency" of the correlation between the two variables. In contrast, if we find that the correlation coefficient is large and the p-value < 0.05 , we will "conclude" that there is a correlation.

The electron-only reconnection in the transition region of the quasi-parallel shock has a strong guide field, as shown in Figs. 2(e) and 3(e) and also in Fig. 6 later, and the outflow velocity is tilted with respect to the current sheet near the X line. Also, most of the electron-only reconnection sites have asymmetric field quantities across the current sheet around each X line, and there is a significant asymmetry in the inflow and outflow velocity patterns. As a result, the outflow velocity parallel to the magnetic field may become significantly large. The parallel outflow component does not contribute to the convection electric field in the reconnection region. In Fig. 5(b), the outflow speed V_{out} may contain a significant contribution from the parallel outflow speed, and it is still not clear whether a large outflow speed makes the reconnection electric field large. Therefore, we investigate another correlation between the reconnection electric field E_r and the convection electric field due to the outflow. If we assume a steady-state reconnection model, where the reconnection electric field is uniform around the X line, the outflow velocity V_{out} will generate the convection electric field $E_z = -(V_{out} \times B)_z/c$, which is equal to the reconnection electric field E_z at the X line. Even though the electron-only reconnection in the shock is not steady-state reconnection, we expect that there is a correlation between E_r and the convection electric field by the outflow. The scatterplot with black data points in Fig. 5(c) shows for E_r as a function of the convection electric field by the outflow. To make this plot, we excluded the data at two X lines where the sign of the convection electric field and the sign of E_z at the X line are opposite; therefore, we used 13 data points. Although there is a large spread of the data points, we see a weak correlation between E_r and the convection electric field. The Spearman's rank correlation coefficient is 0.31. However, again, due to the small sample size, the p-value is 0.30, and

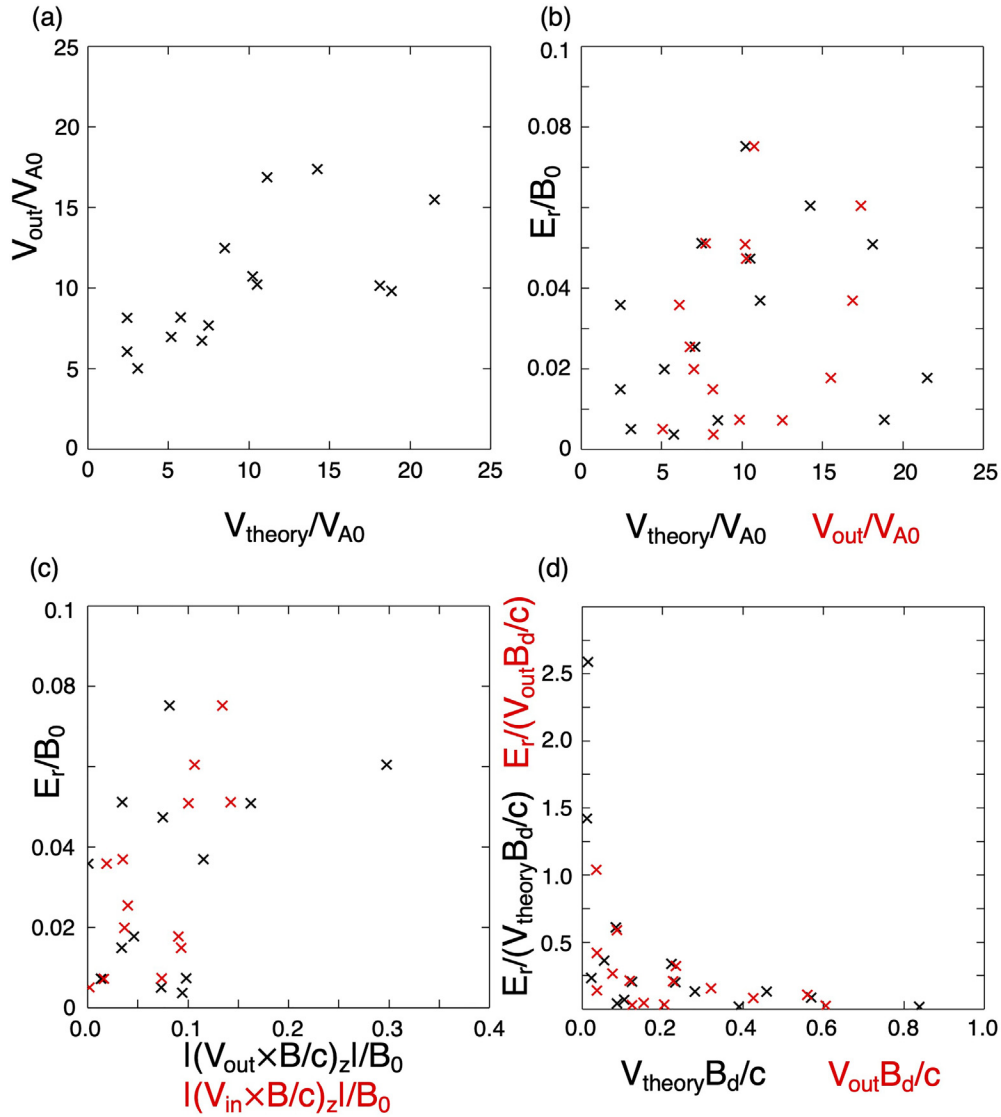


FIG. 5. Scatterplots for electron-only reconnection. (a) V_{out} vs V_{theory} ; (b) E_r vs V_{theory} (black) and E_r vs V_{out} (red); (c) E_r vs convection E_z due to V_{out} (black) and V_{in} (red); and (d) reconnection rate R_t vs $V_{theory} B_d/c$ (black) and R_o vs $V_{out} B_d/c$ (red).

we cannot disprove that there is no correlation. From panels (b) and (c) and the rank correlation coefficients (0.33 for E_r and V_{out} and 0.31 for E_r and the convection electric field), we confirm tendencies that the reconnection electric field E_r is weakly correlated with the outflow V_{out} and the convection electric field, but further study with a larger sample size is necessary. In contrast, the scatterplot with red data points in Fig. 5(c) shows a relation between E_r and the convection electric field due to the inflow velocity. For the inflow velocity, we measured the electron fluid velocity V_{in} at one of the inflow edges of the EDR (the same points where we measure the maxima of B_L along the N axis to obtain B_d), and we computed the z component of the convection electric field $-(V_{in} \times B)_z/c$. We used only 13 data points from reconnection regions where the signs of the convection electric field and the

reconnection electric field are the same. We see a positive correlation between the convection electric field due to the inflow and the reconnection electric field E_r . The positive correlation is seen because the inflow convection generates a roughly uniform electric field in the EDR including the reconnection electric field, even under the turbulent condition (see a quantitative discussion in Sec. III D). The Spearman’s rank correlation coefficient is 0.70, and the p-value is 0.007.

Panel (d) shows a plot for the reconnection rates R_t and R_o . The data points for both rates (black and red) show an increase in the reconnection rate as the normalization quantity (horizontal axis) becomes small. If the reconnection rate were a constant value, we would see a flat distribution of the data points along constant values of R_t and R_o . This plot shows that the reconnection rates are not constant.

The reconnection rates become larger in smaller $V_{theory}B_d/c$ and $V_{out}B_d/c$, because the outflow speed (V_{theory} and V_{out}) becomes small, but the reconnection electric field E_r is only weakly correlated with V_{theory} and V_{out} . Also, the increase is due to small B_d when the size of the reconnection region is small (such as a small sub- d_i scale magnetic island), which makes both B_d and $V_{out} \sim V_{theory}$ small.

Figure 6 shows scatterplots for the reconnection electric field E_r and the reconnection rate R_t as functions of the guide field strength B_g ($|B_z|$ at the X line). In both panels (a) and (b), the black data use the guide field B_g normalized by the upstream magnetic field B_0 , while the red data use B_g normalized by the local value of B_d . In those electron-only reconnection sites, there are generally strong guide fields less than $10B_0$, and if we use a local B_d , the highest guide field is $B_g = 27B_d$, which is due to small B_d in a small reconnection region (small sub- d_i scale island). Panel (a) shows that there is no correlation between the reconnection electric field E_r and the guide field B_g in the black data points. In the red data points, a weak negative correlation is seen between E_r and B_g/B_d , but the highest three B_g/B_d points can be considered outliers, as we explain below. Using the rest 12 red data points (removing the highest three points), the Spearman's rank correlation coefficient is almost zero.

In panel (b), it is also hard to conclude about a correlation between the reconnection rate R_t and the guide field. The highest three reconnection rates ($R_t = 0.6, 1.4,$ and 2.5) show strong guide field $B_g/B_d > 10$, and this is because of the small B_d in a small reconnection region. Therefore, the extremely large reconnection rate R_t for these three X lines can be considered outliers [these three outliers correspond to the three highest R_t in the histogram; Fig. 4(b)], and the other reconnection rates are concentrated in the region less than $R_t < 0.5$. After removing those three outliers of extremely large R_t , there might be a weak negative correlation between the reconnection rate and the guide field strength. The Spearman's rank correlation coefficients are -0.31 (p-value = 0.33) for the black data points and

almost zero for the red data points. R_t shows higher values around 0.35 in $B_g/B_0 < 3$ and $B_g/B_d < 3$, but R_t becomes around 0.1 in the ranges $5 < B_g/B_0 < 10$ and $5 < B_g/B_d < 10$. Tendencies of a weak negative correction are seen in these data points, but the sample size is too small to make a conclusion.

C. Regular reconnection

In the shock transition region, we identified seven regular reconnection sites, indicated by the yellow Xs in Fig. 1(b). We investigated details of the reconnection electric field and ion and electron outflow speeds around these seven X lines. One example of regular reconnection (the X line at $(x, y) = (49.925d_i, 41.825d_i)$, near the largest magnetic island around $x = 50d_i$ and $y = 42d_i$) has already been documented in Ref. 13.

Figure 7 shows field quantities in a regular reconnection site, in the same format as Figs. 2 and 3, except for panel (b), where the white arrows show the ion flow vectors. Around the X line at $(x, y) = (x_X, y_X) = (49.8d_i, 21.2d_i)$, there is a current sheet with negative J_z along the vertical direction [panel (a)]. Across this current sheet, the reconnecting component of the magnetic field reverses its sign. In other words, using the L (direction of the reconnecting magnetic field) and N (normal component) directions drawn in panel (d), we have $B_L > 0$ in $x < x_X$ and $B_L < 0$ in $x_X < x$. The reconnection electric field is negative ($E_z = -0.095B_0$), and the region surrounding the X line has negative E_z [panel (b)].

Panels (c) and (d) show the electron and the ion fluid velocities in the X-line rest frame. The electron flow [panel (c)] shows a bipolar outflow pattern across the X line in the y direction; there is a strong upward outflow $V_{ey} > 0$ in $y_X < y$, while a negative outflow $V_{ey} < 0$ in $y < y_X$. In the $y_X < y$ side, the maximum electron outflow speed reaches $13.0v_A$. However, this outflow speed is much smaller than the predicted electron outflow $V_{e-theory} = 34.9v_{A0}$ using the magnetic

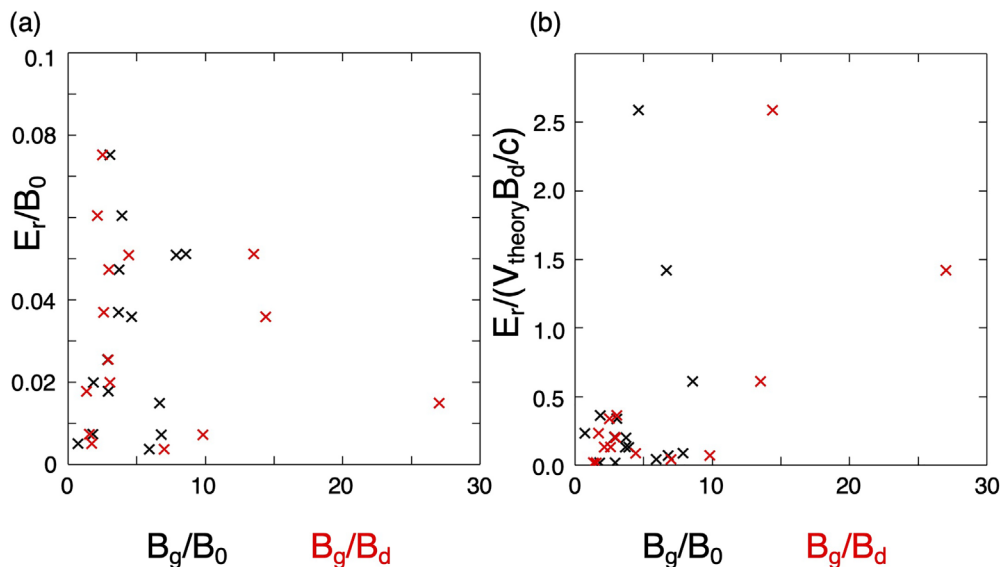


FIG. 6. Scatterplots for electron-only reconnection. (a) E_r vs guide field B_g/B_0 (black) and E_r vs B_g/B_d (red); and (b) reconnection rate R_t vs B_g/B_0 (black) and R_t vs B_g/B_d (red).

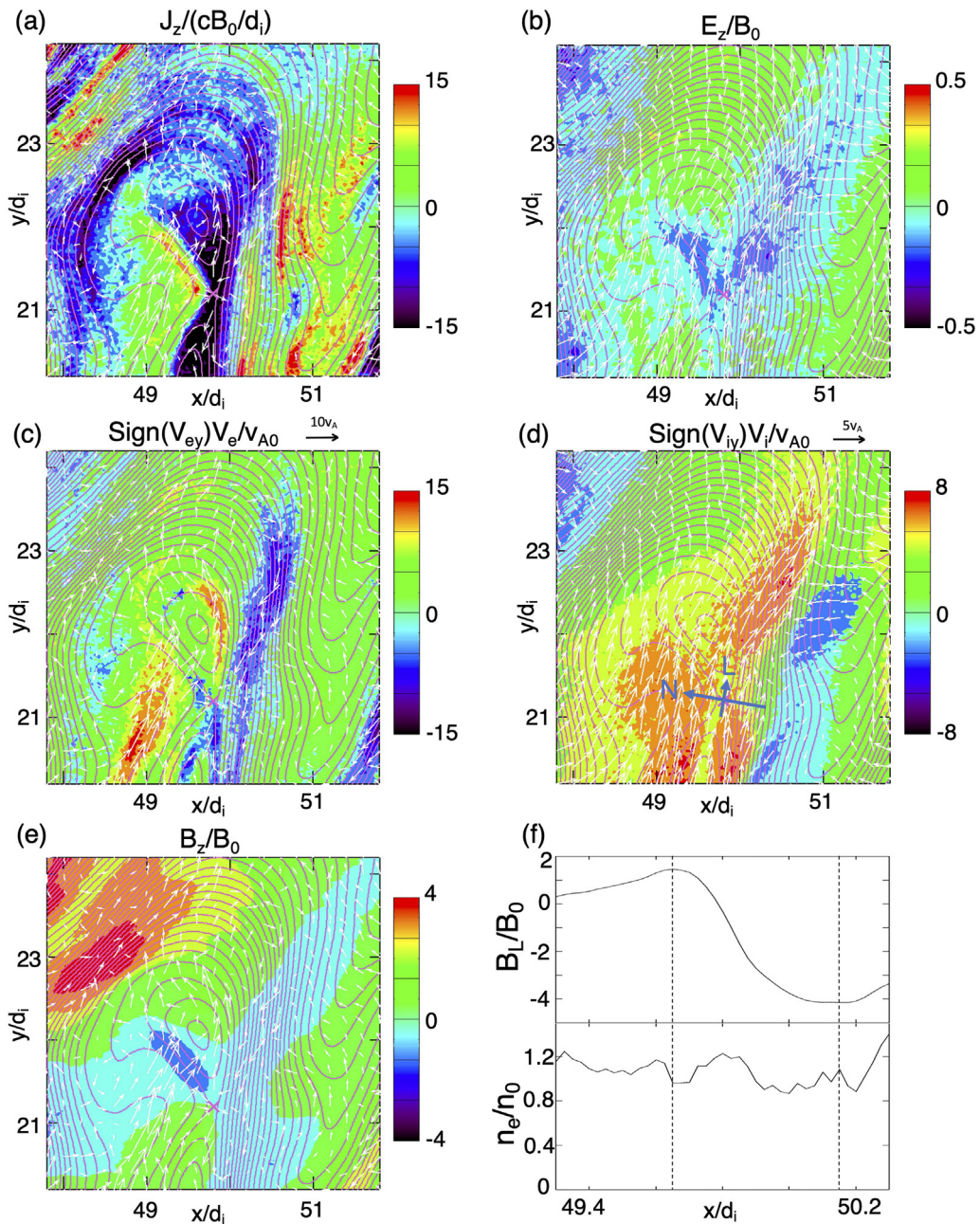


FIG. 7. Field quantities in a regular reconnection site whose X line is at $(x_X, y_X) = (49.8d_i, 21.2d_i)$, in the X-line rest frame, in the same format as in Fig. 2, except for panel (b) where white arrows show the ion fluid velocity vectors in the X-line rest frame.

fields and densities at the two sides [$B_1 = 1.46B_0$, $B_2 = 4.15B_0$, $n_1 = 0.96n_0$, and $n_2 = 1.08n_0$, shown in panel (f)], with the electron mass m_e . Slightly away from the outflow regions, in the region where $x_X < x$ (around $x = 50.5d_i$) and $y_X < y$, there is a strong downward ($V_{ey} < 0$) flow, while in the region where $x < x_X$ (around $x = 49.0d_i$) and $y < y_X$, there is a strong upward ($V_{ey} > 0$) flow. This upward flow is mainly due to another reconnection site at $(x, y) = (48.8d_i, 20.85d_i)$, and the outflow from that neighboring reconnection site

plays a role as a part of the inflow in this regular reconnection site. If we look into the vicinity of the X line at (x_X, y_X) , there is an electron inflow toward the X line from left to right (from the $x < x_X$ side to the $x_X < x$ side). The ion flow [panel (d)] shows a strong upward ($V_{iy} > 0$) flow in both $y < y_X$ and $y_X < y$. In the region $y < y_X$, there are two flows (near $x = 49d_i$ and near $x = 50d_i$) with $V_{iy} > 0$, and the flow near $x = 49d_i$ includes the outflow from the neighboring reconnection site. In the regular reconnection site at (x_X, y_X) , the flow

around $x = 50d_i$ plays a role as the ion inflow. This inflow passes through the X line in the positive y direction, and the flow direction changes to a direction with $V_{ix} > 0$ and $V_{iy} > 0$ in $y_X < y$. The ion outflow has a peak of $7.4 v_{A0}$ at $(x, y) = (50.025d_i, 21.925d_i)$, and another peak of $7.2v_{A0}$ at $(x, y) = (50.6d_i, 22.75d_i)$. Surprisingly, these outflow values are much greater than the predicted ion outflow $V_{i-theory} = 2.5v_{A0}$ using $B_1, B_2, n_1,$ and n_2 with the mass $m_i = 200m_e$. The origin of this unusually fast ion outflow speed is likely the background ion flows due to ion reflection in the shock transition region (see also Ref. 14 for the ion distribution functions that contain reflected ions). Turbulent ion flows in the background already have fast flow speeds, and reconnection in this region further accelerates ions from the X line to the region $y_X < y$. More details of flow structures in this regular reconnection region are given in Figs. S3 and S4 in the [supplementary material](#). Also, Fig. S5 in the [supplementary material](#) shows a Hall electric field in the in-plane electric field, which points toward the magnetic neutral line, due to the decoupling of electron and ion motion.

Note that this regular reconnection site has a few different features from the standard laminar reconnection. One is that the ion outflow is generated in the positive L and negative N side from the X line, but this outflow region near $x = 50d_i$ and $y > 22d_i$ is usually the inflow region in the standard laminar reconnection, where the inflow points toward the X line. This unusual outflow region in this regular reconnection site is produced mainly because of the small size of the magnetic island structure. Another difference is that the ion motion is decoupled from the electron motion in most of the reconnection site around the X line. As a result, the electric field E_z [panel (b)] in the ion exhaust region ($x_X < x$ and $y_X < y$) is not consistent with the convection electric field $-V_i \times B/c$, and the negative sign of E_z in the ion exhaust region is opposite from the positive sign of the convection electric field ($-V_{ix}B_y > 0$ because $V_{ix} > 0$ and $B_y < 0$ in the ion exhaust region). In this ion exhaust region, there is a strong downward ($V_{ey} < 0$ and $V_{ex} < 0$) electron flow [see panel (c) in the region around $x = 50.5d_i$ and $y_X < y$] whose speed is comparable to the ion exhaust speed. Therefore, this decoupling between the electron and the ion motions causes the Hall current, and the generalized Ohm's law tells that E_z is balanced with the convection effect due to the electron motion in the ion exhaust region ($-V_{ex}B_y < 0$ because $V_{ex} < 0$ and $B_y < 0$). This regular reconnection in the shock is very different from the regular reconnection in the Earth's magnetopause/magnetotail, where the convection electric field due to the electron flow and the ion flow show the same sign, and the ion and the electron motions are almost coupled in the ion exhaust region. The reason why there is a strong decoupling between the electron and the ion flows is mainly because the size of the island structure in the shock is small (of the order of d_i), and both ions and electrons with fast flow speeds (of the order of $10 v_{A0}$) cannot be completely magnetized.

Figure 8 shows histograms for the reconnection electric field, the reconnection rates, and the ion and electron outflow speeds in regular reconnection sites. Panel (a) shows the histogram for E_r normalized by the upstream magnetic field B_0 . The reconnection electric fields range from 0 to $0.1B_0$. The mean is $0.039B_0 (= 0.45B_0 \sin \theta V_{sw}/c)$, the minimum is $0.010B_0 (= 0.12B_0 \sin \theta V_{sw}/c)$, and the maximum is $0.095B_0 (= 1.1B_0 \sin \theta V_{sw}/c)$. Comparing with Fig. 3(a) for electron-only reconnection, E_r in regular reconnection in the shock transition region does not have a significant difference from E_r in electron-only

reconnection, and both electron-only reconnection and regular reconnection show similar magnitudes of E_r . Panels (b) and (c) show histograms for reconnection rates, where we chose four normalizations: (1) $B_d V_{e-out}/c$ [panel (b), red], where V_{e-out} is the observed electron outflow speed, (2) $B_d V_{e-theory}/c$ [panel (b), black], (3) $B_d V_{i-out}/c$ [panel (c), red], where V_{i-out} is the observed ion outflow speed, and (4) $B_d V_{i-theory}/c$ [panel (c), black].

Panel (b) shows the reconnection rates $R_{et} = E_r/(V_{e-theory}B_d/c)$ (black) and $R_{eo} = E_r/(V_{e-out}B_d/c)$ (red), based on the electron outflow speeds. Both the black and the red histograms show similar distributions. The mean values are 0.13 (black) and 0.14 (red), the minimum values are 0.018 (black) and 0.028 (red), and the maximum values are 0.35 (black) and 0.29 (red), respectively. Panel (c) shows the histograms for the reconnection rates $R_{it} = E_r/(V_{i-theory}B_d/c)$ (black) and $R_{io} = E_r/(V_{i-out}B_d/c)$ (red) based on the ion outflow speeds. In this plot, the horizontal axis in the bottom (red) is for R_{io} , and the horizontal axis in the top (black) is for R_{it} . For $R_{io} = E_r/(V_{i-out}B_d/c)$, the mean is 0.28, the minimum is 0.058, and the maximum is 0.59. If we multiply a factor of 0.5 with the values of R_{io} in the horizontal axis in panel (c), the distribution of R_{io} looks similar to the distribution of R_{eo} [red curve in panel (b)]. The similarity is because the ion outflow speed reaches a similar value to half the electron outflow speed, as we will see later, which is very different from the ion outflow speed in regular reconnection in the Earth's magnetopause/magnetotail, where the ion outflow speed reaches the Alfvén speed. If we use the theoretical value of the ion outflow speed, $V_{i-theory}$, the reconnection rate R_{it} does not show a value that correctly represents the reconnection rate, because $V_{i-theory}$ is much smaller than the actually observed ion outflow speed, V_{i-out} . The black histogram shows the reconnection rate $R_{it} = E_r/(V_{i-theory}B_d/c)$, based on $V_{i-theory}$. The reconnection rates R_{it} are distributed between 0 and 5.0, which are almost an order of magnitude larger than the reconnection rates R_{io} based on the observed ion outflow speeds.

Panel (d) shows the histograms for the electron outflow speed V_{e-out} (red) and the ion outflow speed V_{i-out} (black). The horizontal axis shown in the bottom (red) is for V_{e-out} , while the horizontal axis shown in the top (black) is for V_{i-out} . The electron outflow speeds range from $10 v_{A0}$ to $20 v_{A0}$. The mean is $14.1 v_{A0}$, the minimum is $11.7 v_{A0}$, and the maximum $19.6 v_{A0}$. The ion outflow speeds range from $4 v_{A0}$ to $10 v_{A0}$. The mean is $7.2 v_{A0}$, the minimum is $4.5 v_{A0}$, and the maximum is $9.6 v_{A0}$. The distribution of V_{i-out} (black) after multiplying a factor of 2.0 with V_{i-out} is similar to the distribution of V_{e-out} (red). These large ion outflows, of the order of $10 v_{A0}$, are much larger than the ion outflow speed (\sim local Alfvén speed) in regular reconnection in the Earth's magnetopause/magnetotail.

Figure 9 shows scatterplots for electron outflow speeds, ion outflow speeds, reconnection electric fields, and reconnection rates. Since the sample size for regular reconnection in this study is too small, we do not perform the correlation analysis, but let us visually check whether there is a tendency of a correlation. Panel (a) shows the electron outflow speed V_{e-out} as a function of $V_{e-theory}$. In contrast with the electron outflow in electron-only reconnection analyzed in Fig. 5(a), the electron outflow V_{e-out} in regular reconnection does not show a positive correlation with $V_{e-theory}$. Instead, the electron outflows in those seven regular reconnection sites show similar values between $10v_{A0}$ and $20v_{A0}$, even in a range of large prediction values around $V_{e-theory} = 30v_{A0}$. Although it is hard to conclude something

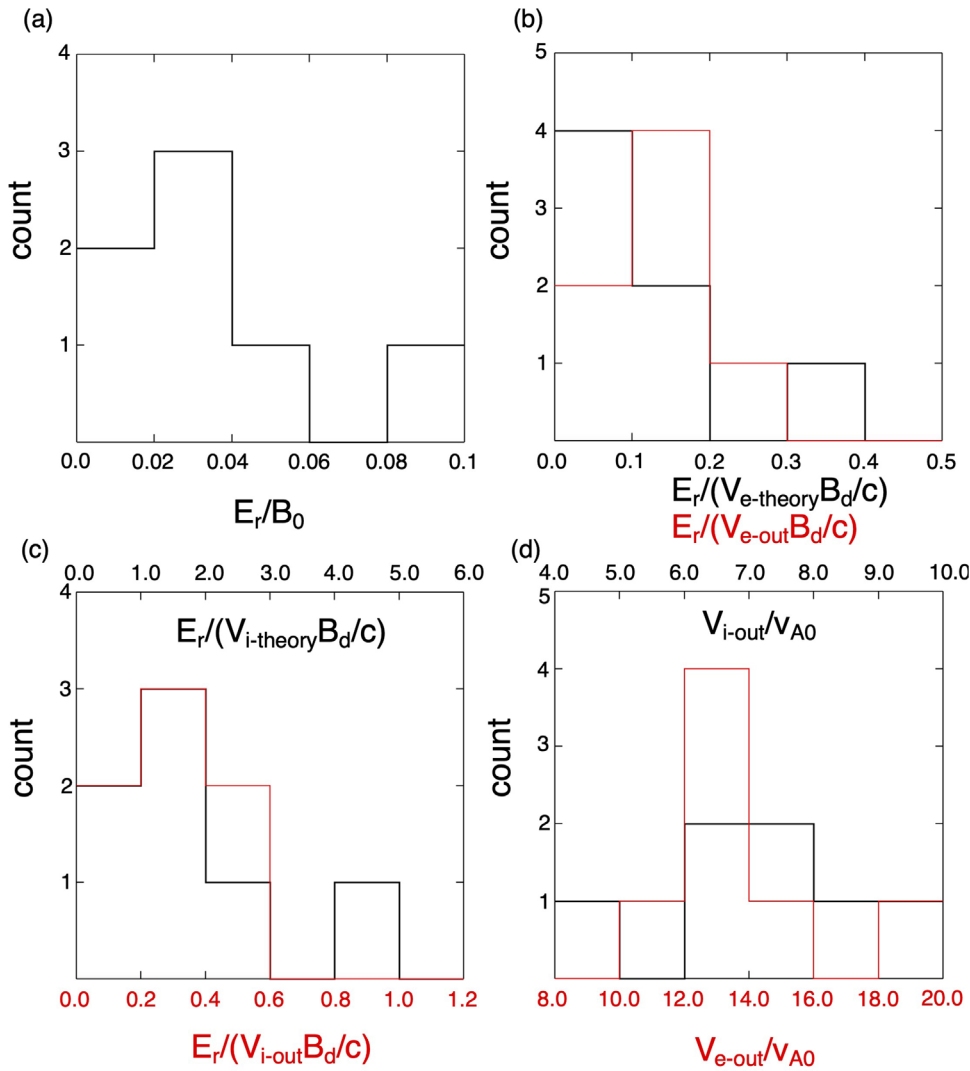


FIG. 8. Histograms for regular reconnection. (a) Reconnection electric field E_r ; (b) reconnection rates $R_{et} = E_r/(V_{e-theory}B_d/c)$ (black) and $R_{eo} = E_r/(V_{e-out}B_d/c)$ (red); (c) reconnection rates $R_{it} = E_r/(V_{i-theory}B_d/c)$ (black) and $R_{io} = E_r/(V_{i-out}B_d/c)$ (red); and (d) ion outflow speed V_{i-out} (black) and electron outflow speed V_{e-out} .

from this small sample size of data, the electron outflow speed seems not greatly affected by the predicted speed.

Panel (b) shows a plot for the ion outflow speed V_{i-out} as functions of the predicted ion speed $V_{i-theory}$ (black) and the observed electron outflow speed V_{e-out} (red). The observed ion outflow speeds V_{i-out} are much larger than the predicted ion outflow speeds $V_{i-theory}$. The values of V_{i-out} are between $4.5 v_{A0}$ and $9.6 v_{A0}$, while the values of $V_{i-theory}$ are between $0.65 v_{A0}$ and $2.5 v_{A0}$. The observed ion outflows V_{i-out} are almost half the observed electron outflow speeds V_{e-out} , between $11.7 v_{A0}$ and $19.6 v_{A0}$. The scatterplot for the red data shows that there is a tendency that the ion outflow speed increases with the electron outflow speed. This fact that V_{i-out} is proportional to V_{e-out} may indicate that the electron outflow speed is determined by the ion outflow speed, which is of the order of the speed of ions reflected by the shock, as explained below.

Regular reconnection sites in the shock transition region are produced after the nonresonant ion-ion beam instability,¹⁴ and the ion

jets in regular reconnection sites reach similar flow speeds as the ions reflected by the shock potential during the instability. Since the speeds of the reflected ions are the same order as the flow speed in the upstream region, which is $9 v_{A0}$ in this shock simulation with $M_A = 11.4$ (see also Figs. 10 and 11 in Ref. 14, where the reflected ions' speeds reach the order of $10 v_{A0}$), the ion jet speeds in those regular reconnection sites reach the same order, around $10 v_{A0}$. Some of regular reconnection sites, such as the site near the largest magnetic island $x = 50 d_i$ and $y = 42 d_i$, clearly show that the peak ion outflow velocity is boosted from the inflow speed with an amount around v_{A0} . In other words, before reconnection, there is already the ion flow with its speed around $10 v_{A0}$ due to the reflected ions, and reconnection generates the ion exhaust with its speed boosted up with an additional speed around v_{A0} . That is why the ion outflow speed in regular reconnection in the shock is of the order of the upstream flow speed (around $10 v_{A0}$ in this study), which is much larger than the ion outflow of the regular reconnection in the Earth's magnetopause/magnetotail. Note that such a

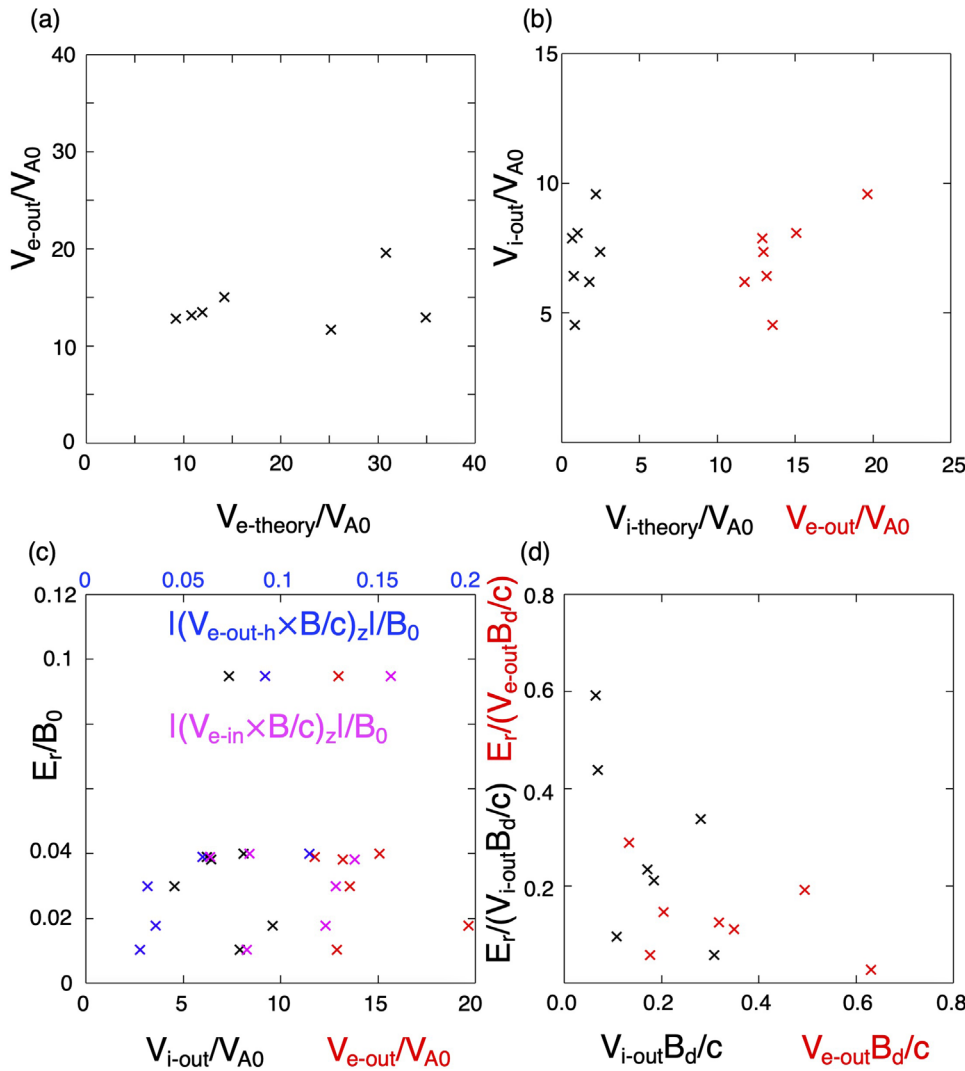


FIG. 9. Scatterplots for regular reconnection. (a) V_{e-out} vs $V_{e-theory}$; (b) V_{i-out} vs $V_{i-theory}$ (black) and V_{i-out} vs V_{e-out} (red); (c) E_r vs V_{i-out} (black), E_r vs V_{e-out} (red), and E_r vs convection E_z by electron outflow (blue) and electron inflow (magenta); and (d) reconnection rates R_{io} vs $V_{i-out}B_d/c$ (black) and R_{eo} vs $V_{e-out}B_d/c$ (red).

boost speed $\sim v_{A0}$ is not regarded as the outflow speed, but we should use the observed outflow speed (V_{i-out}) as the outflow speed. The exact physical reason why the electron outflow speed in the regular reconnection in the shock [panel (a)] does not correlate with the predicted electron speed $V_{e-theory}$ but correlated with the ion outflow speed [panel (b)] still remains to be investigated, but this may be because the electron outflow is induced by the ion outflow to reduce the charge separation produced by the strong ion flows in those reconnection sites.

Panel (c) shows the reconnection electric field E_r as functions of V_{i-out} (black) and V_{e-out} (red), as well as the convection electric field E_z (blue) due to the electron outflow. These data show that E_r is correlated with neither V_{i-out} nor V_{e-out} . However, E_r shows a correlation with the convection electric field. We note that the convection electric field shown here is not the one at the point of the maximum electron outflow, but we chose the midpoint between the X line and the point of the maximum electron outflow, and then computed the convection $E_z = -(\mathbf{V}_{e-out-h} \times \mathbf{B})_z/c$ at the midpoint (where $\mathbf{V}_{e-out-h}$

represents the electron flow velocity at the midpoint). This is because the signs of the convection electric fields by the electron maximum outflows are opposite from those of the reconnection electric fields in four sites out of seven regular reconnection sites [Fig. 7(b) is an example]. However, the reconnection electric field E_r should be related to the convection E_z at a certain point of the outflow region, between the X line and the maximum position of the outflow. For example, in Fig. 7(b), E_z near the X line is negative because of the negative convection electric field due to the electron flow, even though the convection E_z at the position of the maximum electron outflow becomes positive. The convection E_z due to the ion flow is also negative near the X line, but due to the motion separation between the electron and ion, the convection E_z by the electron should be taken into account. For this reason, we investigate the convection electric field at the midpoint between the X line and the position of the maximum electron outflow. In panel (c), the blue data points show E_r as a function of the convection electric field E_z by the electron at the midpoint. Here, we only used six points, because in one region, the sign of the convection E_z is

opposite to E_z at the X line. The blue data points clearly show an increase trend of E_r as the convection E_z increases. This result indicates that the reconnection electric field is explained by the convection E_z due to the electron flow, and the reconnection electric field E_r in regular reconnection in the shock is the same order as that in electron-only reconnection, because in both types of reconnection, the electron outflow speed is the same order. The magenta data points show the relation between E_r and the convection E_z due to the electron inflow velocity, $E_z = -(\mathbf{V}_{e-in} \times \mathbf{B})_z/c$, and we also see an increase trend of E_r as the convection E_z increases.

Panel (d) is for the reconnection rates $R_{io} = E_r/(V_{i-out}B_d/c)$ and $R_{eo} = E_r/(V_{e-out}B_d/c)$ as functions of $V_{i-out}B_d/c$ (black) and $V_{e-out}B_d/c$ (red), respectively. Similar to the result in electron-only reconnection [panel (d) in Fig. 5], both reconnection rates R_{io} and R_{eo} are not constant, but they increase when $V_{i-out}B_d/c$ and $V_{e-out}B_d/c$ become small.

Figure 10 shows scatterplots for the reconnection electric field and reconnection rates as functions of two normalized guide fields, B_g/B_0 and B_g/B_d . Panel (a) shows a plot for E_r as functions of B_g/B_0 (black) and B_g/B_d (red). Both data show that there seems to be no correlation between the reconnection electric field E_r and the guide field B_g . Panel (b) shows reconnection electric fields R_{io} and R_{eo} as functions of B_g/B_0 (black) and B_g/B_d (red). Data of both types of outflows (V_{e-out} and V_{i-out}) are represented by different symbols (cross: the electron outflow V_{e-out} , and diamond: the ion outflow V_{i-out}). Again, there seems no correlation between the reconnection rates and the guide field strength. If we look into more details of the dependences of E_r , R_{io} , and R_{eo} , we see that E_r , R_{io} , and R_{eo} in the regions $1 \leq B_g/B_0 \leq 2.5$ and $1 \leq B_g/B_d \leq 2.5$ show larger values than those in higher guide fields. Therefore, there may be weak negative correlations between E_r , R_{io} , and R_{eo} and the guide field strengths. However, it is hard to conclude the dependence using such a small sample size of data.

D. Discussions for the outflow speed and the reconnection electric field in shocks

Let us discuss first the outflow speed in electron-only reconnection in a shock. We have confirmed that the electron outflow speed V_{out} is well correlated with V_{theory} , which is close to the local electron Alfvén speed, using the asymmetric reconnection theory in Ref. 20. In the theory, it is assumed that there are two-sided outflow jets across the X line in the L direction (the direction of the reconnecting magnetic field). However, in the shock we investigated, there are many electron-only reconnection sites that show one-sided electron jets; therefore, it is not obvious why the same theory with two-sided outflows can be applied to those one-sided electron outflows. In the following, we will argue that the theory can be applied to both the two-sided outflow case and the one-sided outflow case.

To derive the outflow speed, the asymmetric reconnection theory uses the mass conservation law, the energy conservation law, and the uniform reconnection electric field. The mass and energy conservations for the two-sided outflow case are written as follows [the same as Eqs. (10) and (11) in Ref. 20, replacing the ion mass with the electron mass]:

$$l(m_e n_1 v_{in1} + m_e n_2 v_{in2}) = 2\delta m_e n_{out} V_{out}, \tag{1}$$

$$l\left(\frac{B_1^2}{8\pi} v_{in1} + \frac{B_2^2}{8\pi} v_{in2}\right) = 2\delta\left(\frac{1}{2} m_e n_{out} V_{out}^2\right) V_{out}, \tag{2}$$

where l is the half length of the diffusion region [the distance from the X line at $L=0$ to the end point of the diffusion region in the L direction; see the diagram in Fig. 11(a)]; v_{in1} and v_{in2} are the inflow speed in region 1 and that in region 2, respectively. Region 1 has $|B_L| = B_1$ and $n_e = n_1$, while region 2 has $|B_L| = B_2$ and $n_e = n_2$. In the outflow region, the density becomes $n_e = n_{out}$. Note that the theory in Ref. 20 assumes quasi-steady reconnection and neglects the time derivative in

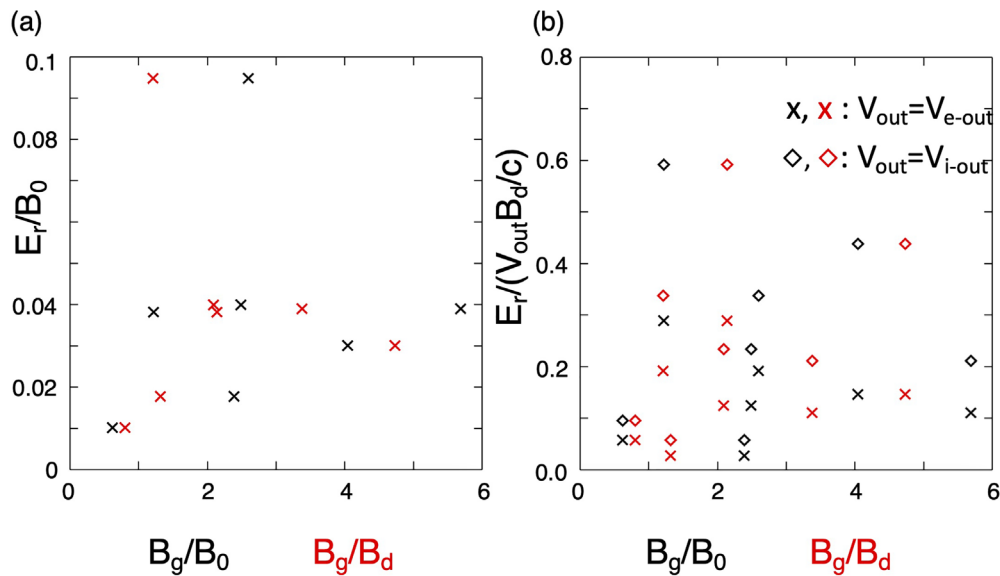


FIG. 10. Scatterplots for regular reconnection. (a) E_r vs guide field B_g/B_0 (black) and E_r vs B_g/B_d ; and (b) reconnection rates R_{io} and R_{eo} vs B_g/B_0 (black) and R_{io} and R_{eo} vs B_g/B_d (red).

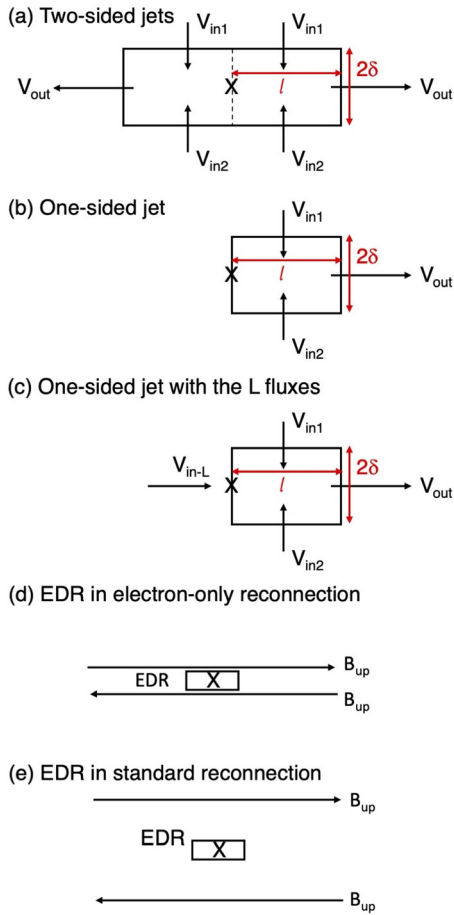


FIG. 11. Schematic diagrams: (a) two-sided jets, (b) one-sided jet, (c), one-sided jet with the L fluxes, (d) EDR in electron-only reconnection, and (e) EDR in standard reconnection. In each plot, the X line is denoted by the X mark. In (d) and (e), B_{up} is the magnetic field in the upstream regions.

the theory. We can justify applying the theory to electron-only reconnection even in a turbulent case, because the timescale of the electron-only reconnection observed in the simulation is tens of Ω_e^{-1} (see Fig. 2 in Ref. 13, which shows electron-only reconnection lasted longer than $0.25\Omega_i^{-1} = 50\Omega_e^{-1}$ for the mass ratio 200), while the electron transit time in the reconnection region can be estimated as $l/V_{out} \sim d_i/v_{Ae} \sim 10\Omega_e^{-1}$, which is shorter than the reconnection timescale. Therefore, during this short transit time, the field structure does not change a lot, and a quasi-steady state can be assumed in electron-only reconnection. We also assume that the reconnection electric field is uniform, and we have

$$v_{in1}B_1 = v_{in2}B_2. \quad (3)$$

Using these three equations, we have the outflow speed V_{out} as

$$V_{out} = \left(\frac{B_1B_2}{4\pi m_e n_1B_2 + n_2B_1} \right)^{1/2} = V_{theory}, \quad (4)$$

where we use the notation V_{theory} , and this is the hybrid version of local electron Alfvén speed in asymmetric reconnection.

Looking into the derivation of this outflow speed V_{out} , we found that although the inflows pass through the positive N side and the negative N side of the diffusion region with its length $2l$, we consider only half the region, such as the region $0 < L$, and the mass and energy fluxes that pass the X line at $L = 0$ from the other side ($L < 0$) are zero. This is because we are considering the two-sided outflows that are symmetric across the X line in the L direction, and as long as the system is symmetric, we do not have to consider the other L side of the diffusion region. This means that in such a situation where there are no mass and energy fluxes in the L direction across the X line, we can discuss a one-sided outflow. Comparison between the two-sided outflow case and the one-sided outflow case is shown in Figs. 11(a) and 11(b). Even when there are L -directional fluxes that pass through the X line, if we can neglect those fluxes, we have the same outflow speed as Eq. (4).

However, in the simulation, we identified regions where there are strong L -directional fluxes across the X line. For example, in Fig. 2(c), we see that there is a strong electron inflow passing through the X line from the positive L side along the positive J_z region. This L -directional flow is due to the background flow in the shock turbulence. In this case, we cannot directly apply the theory to this region. Instead, let us include such L -directional fluxes as follows [see also the diagram in Fig. 11(c)]:

$$l(m_e n_1 v_{in1} + m_e n_2 v_{in2}) + 2\delta m_e n_{in-L} v_{in-L} = 2\delta m_e n_{out} V_{out}, \quad (5)$$

$$\begin{aligned} l \left(\frac{B_1^2}{8\pi} v_{in1} + \frac{B_2^2}{8\pi} v_{in2} \right) + 2\delta \left(\frac{1}{2} m_e n_{in-L} v_{in-L}^2 \right) v_{in-L} \\ = 2\delta \left(\frac{1}{2} m_e n_{out} V_{out}^2 \right) V_{out}, \end{aligned} \quad (6)$$

where in the left-hand sides of the equations above, we included the mass flux and energy flux (see the second term in each equation) with its density n_{in-L} and speed v_{in-L} . Here, we assume that the density n_{in-L} in the inflow side is different from the density in the outflow side n_{out} , because there is asymmetry in the L direction across the X line. Note that in this formulation, flows are in the X-line rest frame, and V_{out} represents the total flow velocity in the outflow direction, which is the sum of the background flow and the flow produced by reconnection in the X-line rest frame. From these equations, we obtain V_{out} as follows:

$$V_{out} = \left(\frac{B_1B_2}{4\pi m_e n_1B_2 + n_2B_1} \right)^{1/2} \left[\frac{1 - (n_{in-L}/n_{out})(v_{in-L}/V_{out})}{1 - (n_{in-L}/n_{out})(v_{in-L}/V_{out})^3} \right]^{1/2}, \quad (7)$$

where we assume that $n_{in-L} \leq n_{out}$ and $v_{in-L} \leq V_{out}$ to make the outflow speed a real number. Since the right-hand side contains the ratio v_{in-L}/V_{out} , this is not an explicit expression of V_{out} . To obtain the explicit expression of V_{out} , we need another equation that has a relation between n_{in-L} and n_{out} ; however, we can discuss the characteristics of the outflow speed, in particular, the dependence on the ratio of v_{in-L}/V_{out} using Eq. (7). When the inflow speed is negligibly small, $v_{in-L} \ll V_{out}$, which corresponds to the case where we neglect the L -directional fluxes in the two equations, we obtain $V_{out} \sim V_{theory}$. Also, in a case where v_{in-L} is large enough and close to V_{out} (i.e., $v_{in-L} \rightarrow V_{out}$), as in Fig. 2(c), the outflow speed becomes $V_{out} \sim V_{theory}$. The outflow V_{out} becomes slightly smaller than V_{theory} when v_{in-L} is

neither small nor large, that is, $0 \ll v_{in-L} < V_{out}$. For example, when we assume that $v_{in-L} = 0.5V_{out}$ and $n_{in-L} = n_{out}$, the outflow speed $V_{out} \sim 0.75V_{theory}$. The outflow speed V_{out} is of the order of V_{theory} . In the Appendix, V_{out} is discussed more precisely as a function of v_{in-L} and n_{in-L}/n_{out} , and it is shown that V_{out} is of the order of V_{theory} .

Next, let us discuss the magnitude of the reconnection electric field in shocks, by comparing with that in the standard laminar reconnection in the Earth's magnetopause/magnetotail. In the shock, we observed that the reconnection electric field E_r is of the order of $0.1B_dV_{out}/c$ in electron-only reconnection, where V_{out} is close to V_{theory} , which is close to the local electron Alfvén speed. At a first glance, this is similar to the reconnection electric field $E_r \sim 0.1B_{de}v_{Ae}/c$ in the standard laminar reconnection in the magnetopause/magnetotail, where B_{de} is the magnetic field at the edge of the EDR, and v_{Ae} is based on B_{de} . However, there is a significant difference between E_r in a shock and E_r in the standard laminar reconnection. In electron-only reconnection, since the reconnection region is small and the current sheet thickness is sub- d_i scale (several electron skin depth d_e), the upstream magnetic field B_{up} rapidly decreases to the X line within such a small scale of several d_e . In other words, the current density in this region becomes significantly large due to large $\partial B_L/\partial N \propto B_{up}/d_e$. Therefore, the EDR occupies almost the entire reconnection region, and B_d [reconnecting magnetic field, $B_d = 2B_1B_2/(B_1 + B_2)$] is close to the upstream magnetic field B_{up} . See the diagram in Fig. 11(d).

In contrast, in the standard laminar reconnection, since the reconnection involves both ions and electrons, there is a scale separation between the ion and electron motions, and the EDR, which has a thickness of several d_e , is embedded in the ion diffusion region (IDR), which has a thickness of several d_i . See the diagram in Fig. 11(e). The current density is of the order of B_{up}/d_i , which is smaller than the current density in electron-only reconnection. In the standard laminar case, reconnection can be discussed based on the IDR, and the reconnecting magnetic field near the edge of the IDR is close to B_{up} . We have a reconnection electric field $E_r \sim 0.1B_{up}v_A/c$, where v_A is the Alfvén speed based on B_{up} . The EDR is located in the vicinity of the X line, where the electron outflow is generated and reaches v_{Ae} based on the magnetic field B_{de} at the edge of the EDR. The reconnection electric field is uniform inside the EDR and the IDR. Therefore, the relation $E_r \sim 0.1B_{de}v_{Ae}/c \sim 0.1B_{up}v_A/c$ holds, and the reconnection electric field in the standard laminar reconnection is eventually $E_r \sim 0.1B_{up}v_A/c$. Comparing the reconnection electric field $E_r \sim 0.1B_{up}v_{Ae}/c$ in electron-only reconnection with the reconnection electric field $E_r \sim 0.1B_{up}v_A/c$ in the standard laminar reconnection, we found that E_r in electron-only reconnection is $(m_i/m_e)^{1/2}$ times larger. This is because of the difference in the magnetic field B_d in electron-only reconnection and B_{de} in the standard reconnection, $B_{de} \ll B_d$. The fact that a large reconnection electric field is generated in electron-only reconnection was first reported in a PIC simulation study in Ref. 12, and our result is consistent with that study.

In regular reconnection in the shock, we observed that reconnection proceeds with fast outflow speeds in both electrons and ions, of the order of $10 v_{A0}$. The simulation shows that $V_{i-out} \sim 0.5V_{e-out}$. However, ions are mostly unmagnetized in the entire reconnection region, and reconnection regions almost resemble electron-only reconnection sites, in which electron outflows generate reconnection electric fields. In regular reconnection sites in the shock, the diffusion region is almost like the EDR, and there seems to be no IDR boundaries beyond

which ions are magnetized, since the current sheet thickness ($\sim 0.5d_i$) is too small, even though ions are involved and accelerated to form an outflow jet. The plots of $E'_{z-e} = [\mathbf{E} + \mathbf{V}_e \times \mathbf{B}/c]_z$ and $E'_{z-i} = [\mathbf{E} + \mathbf{V}_i \times \mathbf{B}/c]_z$ are shown in Figs. S3 and S4 in the supplementary material, and regions with nonzero values of $|E'_{z-e}|$ and $|E'_{z-i}|$ are where electrons and ions are unmagnetized, respectively. Regions with nonzero $|E'_{z-e}|$ roughly correspond to the current sheet, indicating that the EDR is covering the reconnection region. In contrast, regions with nonzero $|E'_{z-i}|$ spread beyond the reconnection region. These ions in the jet are not magnetized, and the generalized Ohm law tells that the electron convection term $-\mathbf{V}_e \times \mathbf{B}/c$ generates the convection electric field. Therefore, reconnection is likely controlled by electron outflows, instead of the ion outflows, and reconnection behaves like electron-only reconnection. We confirmed that the reconnection electric field E_r in regular reconnection in the shock is the same order as E_r in electron-only reconnection. Therefore, the reconnection electric field in regular reconnection is also $E_r \sim 0.1B_dV_{e-out}/c$, and this is larger than the standard laminar reconnection, since V_{e-out} is of the order of $10 v_{A0}$.

IV. MMS OBSERVATION OF ELECTRON JETS IN ELECTRON-ONLY RECONNECTION

Figure 12 shows an observation of electron-only reconnection in the Earth's magnetosheath downstream of a quasi-parallel shock, measured by the MMS 1 spacecraft on December 9, 2016, which shares similarities with the simulation events. More electron-only reconnection events in the magnetosheath are shown and analyzed in Ref. 7. In this event, MMS spacecraft were located at approximately $[11, 3, 0.3]R_E$ in GSE coordinates, where R_E is the Earth radius. Magnetic fields are measured by the flux gate magnetometer,²⁷ electric fields are measured by the electric field double probes,^{28–30} and the plasma data are from the fast plasma investigation.³¹ During this interval, MMS passed through a current sheet, indicated by the magnetic field reversal in B_L [panel (b)], which changes from negative to positive values across the current layer, marked by the two vertical dashed lines. We define the LMN coordinate system based on a hybrid minimum variance analysis³² on the magnetic field over the time interval December 9, 2016/09:03:29.0706 to December 9, 2016/09:03:29.2464, as $\hat{\mathbf{N}} = \hat{\mathbf{b}}_1 \times \hat{\mathbf{b}}_2$, $\hat{\mathbf{M}} = \hat{\mathbf{x}}_{\max} \times \hat{\mathbf{N}}$, and $\hat{\mathbf{L}} = \hat{\mathbf{M}} \times \hat{\mathbf{N}}$, where $\hat{\mathbf{b}}_1$ and $\hat{\mathbf{b}}_2$ are the magnetic field direction on either side of the interval, and $\hat{\mathbf{x}}_{\max}$ is the maximum variance direction of the magnetic field. Inside the interval of the current layer, B_L shows a local minimum value -5 nT, and after MMS exited the current layer, it gradually increases to 10 nT. The B_M field is around -40 nT before MMS passed through the current sheet, and it increases to -20 nT after the current layer. The normal magnetic field B_N is always small, and it reduces from 3 nT to almost zero (a small negative value) during the current sheet crossing. The electron density [panel (a)] is around 14 cm^{-3} before MMS entered the current sheet, and it slightly increases in the current layer. The density is around $15\text{--}16 \text{ cm}^{-3}$ after the current layer, and it further increases to 22 cm^{-3} near the end of the shown interval.

During this current sheet crossing, MMS 1 detected a bipolar V_{eL} [panel (c)], which shows both positive (around 580 km/s) and negative (around -170 km/s) peaks. The velocity V_{eM} [panel (d)] has a negative peak near the B_L reversal point (vertical dotted line), and the speed reaches 1000 km/s. The velocity V_{eN} [panel (e)] also shows a positive peak 200 km/s, but V_{eN} is near zero at the V_{eL} maximum. Therefore, the maximum in-plane speed $(V_{eL}^2 + V_{eN}^2)^{1/2}$ is around 580 km/s.

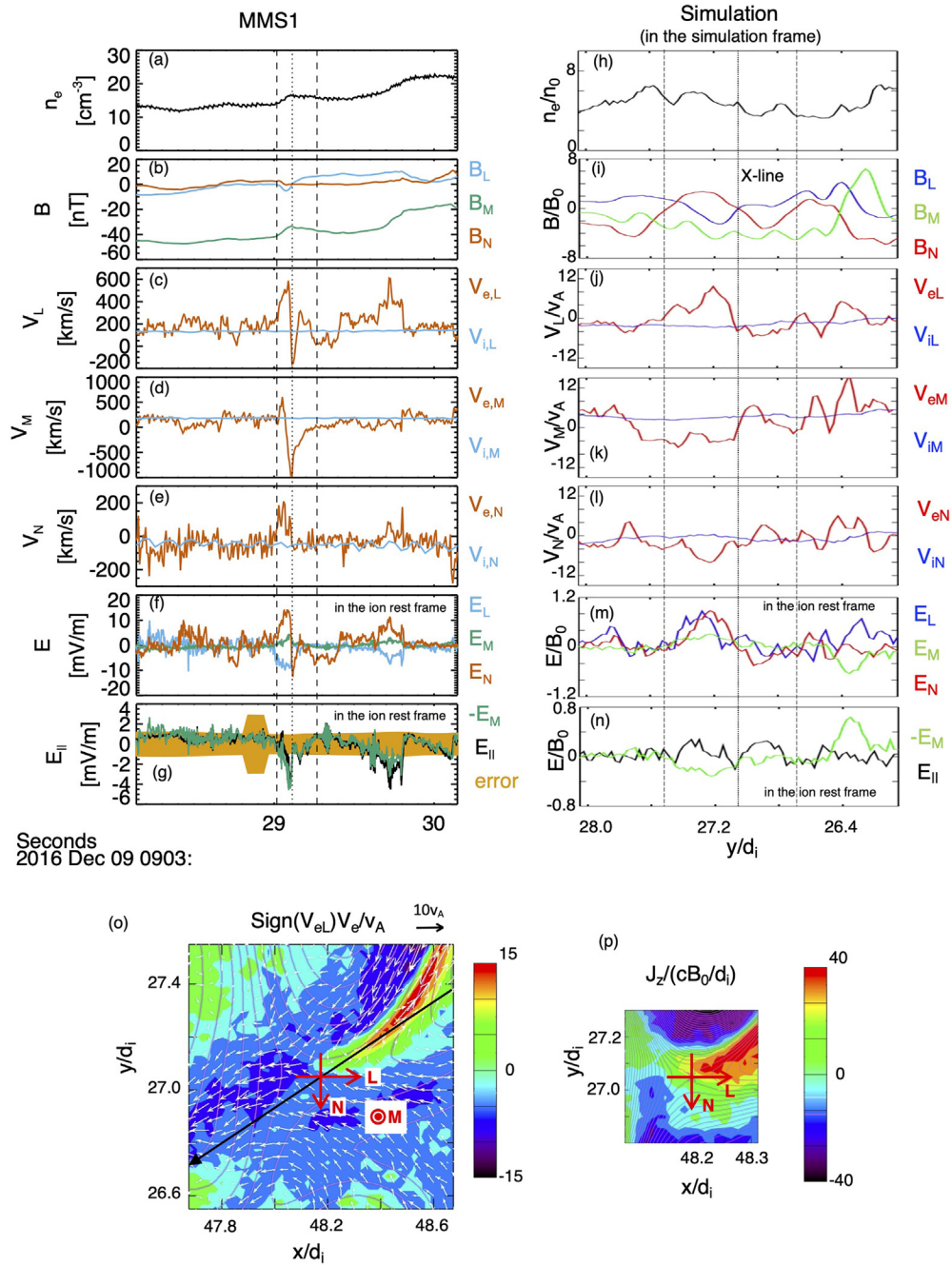


FIG. 12. (a)–(g) MMS observation data for electron-only reconnection: (a) electron density, (b) magnetic fields, (c)–(e) fluid velocities, (f) electric fields, and (g) parallel electric field and $-E_M$. The vertical dashed lines show the region a current sheet, and the dotted line indicates the B_L reversal. (h)–(n) Simulation data, the same quantities as in (a)–(g). (o) 2D plot of the in-plane electron fluid speed in the simulation frame. The black line is where the quantities in (h)–(n) are plotted. White arrows show the vectors of the electron fluid velocity, and (p) 2D plot of the current density J_z .

Based on the B_L field ~ -5 nT and the density $\sim 16 \text{ cm}^{-3}$ when B_L takes the local minimum value inside the current layer, the Alfvén speed is 27 km/s, and the maximum V_{eL} (~ 580 km/s) corresponds to 22 times the Alfvén speed. Since there is a background flow around

140 km/s in the L direction (see the value of V_{iL} in blue), the difference between the peak speed and the background is 440 km/s, which is 16 times the Alfvén speed. These flow speeds are smaller than the electron Alfvén speed (43 times the Alfvén speed), but they almost reach

half the electron Alfvén speed. In contrast, ion fluid velocities show almost uniform velocities, and no jets are recognized. Based on these data (the bipolar outflows in V_{eL} collocated with the B_L reversal, the V_{eM} peak near the B_L reversal, and no ion outflows), we conclude that electron-only reconnection occurs in this current sheet.

Panels (f) and (g) show electric fields in the frame moving with the average ion fluid velocity, that is, $\mathbf{E}_{sc} + \mathbf{U}_{i0} \times \mathbf{B}$, where \mathbf{E}_{sc} is the electric field in the spacecraft frame, and \mathbf{U}_{i0} is the ion fluid velocity averaged over $10d_i$ surrounding the event. This reference frame assumes the reconnecting current sheet (including the X line) is being advected in the background plasma flow. This assumption appears to be broadly consistent with the current sheet velocities obtained for a survey of magnetosheath reconnection events in Ref. 7 when compared to the N -component of the velocity, which could be obtained from multispacecraft timing analysis. Panel (f) shows that there is a bipolar E_N structure in the current sheet, and E_M enhances at the B_L reversal point (dotted line), which is considered to be the vicinity of the X line, up to around 4 mV/m. This E_M is considered to be close to the reconnection electric field. Panel (g) shows that the parallel electric field E_{\parallel} has a negative value close to the value of $-E_M$ at the B_L reversal point, owing to the large guide field in the event. This large $|E_{\parallel}|$ during the crossing of the current sheet is consistent with another observation of guide-field reconnection in the magnetosheath.³³ The value of $|E_M|$ at the B_L reversal point, 4 mV/m, is larger than the uncertainty of measurements (orange curve).

The right panels (h)–(n) show a simulation result of electron-only reconnection, the same quantities as in the MMS observation [panels (a)–(g)]. This electron-only reconnection site has been analyzed in our previous paper,¹³ which shows two-sided electron jets around the X line at $(x, y) = (48.175d_i, 27.05d_i)$. The in-plane electron fluid velocity $\mathbf{V}_e = (V_{ex}^2 + V_{ey}^2)^{1/2}$ in the simulation frame is shown in panel (o), where the coordinates L and N are indicated by the red arrows around the X line. We determined the L and N directions based on the orientations of the current sheet and the magnetic field lines near the X line. Panel (p) shows a region around the X line, in the same scale as in panel (o): The color shows the current density J_z and the magenta lines are the contours of the vector potential A_z , representing field lines. Based on the field line orientation, we visually determined the L and N directions, and the M direction is the same as the z direction. The quantities shown in panels (h)–(n) are the values along the black straight line in panel (o), which mimics a spacecraft trajectory, and the horizontal axis in each plot in panels (h)–(n) represents the y coordinate along the black line [note that y increases from right to left in panels (h)–(n)]. We tried several line trajectories in the simulation, and this straight line in panel (o) is one of the trajectories that show consistency in the quantities between the simulation and the observation. The two vertical dashed lines in (h)–(n) indicate the region with the bipolar electron outflows in V_{eL} , and the dotted line represents the position of the X line. Since we focus only near the reconnection region in the simulation, the interval between the two dashed lines in (h)–(n) is more expanded than the corresponding interval in (a)–(g) in the observation. Note that panels (h)–(l) show the quantities in the simulation frame (where the X line is moving) to compare with the observation data [panels (a)–(e)] in the spacecraft frame, and panels (m) and (n) show the electric fields in the ion rest frame (using $\mathbf{E} + \mathbf{V}_{iX} \times \mathbf{B}/c$, where $\mathbf{V}_{iX} = [-2.6, 0.64, 3.2]v_{A0}$ is the ion fluid velocity at the X line), to compare with the observation data

[panels (f) and (g)] in the ion rest frame. These electric fields in panels (m) and (n) are close to the electric fields in the X-line rest frame (not shown). Also, the reconnection electric field E_M at the X line is frame-independent.

The magnetic field B_L [panel (i)] reverses at the X line, and the electron velocity V_{eL} [panel (j)] shows anticorrelation with B_L . Along the black line in (o), panel (j) shows that the positive V_{eL} outflow speed becomes $\sim 10v_A$ at $y = 27.2d_i$, while the negative V_{eL} peak is $\sim -5v_{A0}$ at $y = 26.9d_i$. The velocity V_{eM} [panel (k)] becomes $-4v_{A0}$ in the region of the positive V_{eL} side, including the X line, but it becomes near zero in the negative V_{eL} side. This shift of the negative V_{eM} toward the positive V_{eL} region indicates that the current sheet ($J_z > 0$) is slightly offset toward the negative B_L region [see also the 2D plot of J_z in panel (p)], which is not observed in the MMS V_{eM} plot, and this is possibly caused by turbulent flows around the X line. The velocity V_{eN} [panel (l)] shows a negative value in the region of positive V_{eL} , and the peak outflow speed $(V_{eL}^2 + V_{eN}^2)^{1/2}$ becomes much larger in the negative B_L side than the other side. Note that we can confirm in panel (o), where the vector arrows show the direction of the flow, that the vector arrows near the positive V_{eN} peak ($y \sim 26.9d_i$) and the negative V_{eN} peak ($y \sim 27.2d_i$) are in the outflow direction, not in the inflow direction. Therefore, we consider that $(V_{eL}^2 + V_{eN}^2)^{1/2}$ represents the outflow speed in those peak positions. Ion flows do not show jet structures, and they are almost constant.

The electric field E_N [panel (m)] shows a bipolar structure in the current sheet, and the correlation between E_N [panel (m)] and V_{eL} [panel (j)] is consistent with the observation [panels (f) and (c)]. In contrast, the sign of E_L at the positive E_N peak near $y = 27.2d_i$ is positive, which is opposite from the negative sign of E_L at the positive E_N in the observation [panel (f)]. The electric field $E_L(> 0)$ in this region in the simulation is consistent with the sign of $-\mathbf{V}_e \times \mathbf{B}$, and mainly due to the negative V_{eN} and the negative B_M . If the flow V_{eN} were positive as in the observation, E_L would be negative in this region.

The E_M field [panel (m)] shows a positive value, around $0.06B_0$, at the X line, and this value is close to $0.1B_d V_{out}/c$, where $B_d = 1.8B_0$ and $V_{out} = 18v_A$ [note that B_d and V_{out} are the values used in the analysis in Sec. III B, not the values along the black line in panel (o)]. In panel (n), the parallel electric field E_{\parallel} shows a negative value at the X line (dotted vertical line), consistent with the negative value of $-E_M$, because of the negative B_M and the positive E_M at the X line.

If we compare these panels (h)–(n) obtained in the simulation with the MMS observation data (a)–(g), we see similarities between them. The B_L reverses from negative to positive (from $-3B_0$ to $2B_0$ in the simulation, but from -5 to 10 nT in the observation). The magnitude of B_M is large in the current sheet ($B_M \sim -5B_0$ in the simulation, but $B_M \sim -40$ nT in the observation). The velocity V_{eL} reverses near the B_L reversal (from $10v_{A0}$ to $-5v_{A0}$ in the simulation, but from 580 to -150 km/s in the observation), and V_{eM} shows a negative peak in the current sheet ($V_{eM} = -4v_{A0}$ in the simulation, and $V_{eM} = -1000$ km/s in the observation). Note that $10v_{A0}$ in the simulation corresponds to 70% of the electron Alfvén speed $v_{Ae} = 14.4v_{A0}$ based on the mass ratio $m_i/m_e = 200$, and both the simulation ($10v_{A0} \sim 0.7v_{Ae}$) and the observation (580 km/s $\sim 0.5v_{Ae}$) show the same order. In addition, the electric field E_N shows a bipolar structure (changing from $0.8B_0$ to $-0.4B_0$ in the simulation, but from 14 to -13 mV/m in the observation). The reconnection electric field E_M is a positive value ($0.06B_0$ in the simulation, while 4 mV/m in the

observation), much weaker than the peak value of E_N . In addition, the parallel electric field E_{\parallel} is consistent with a negative value of $-E_M$ in both simulation and observation. Therefore, it is possible that the MMS trajectory is similar to the black straight line that crosses the X line.

However, there are also differences between the observation and the simulation. In the observation, the density increases across the current sheet from 13 to 17 cm^{-3} , while the simulation shows a decrease from $6n_0$ to $4n_0$ across the V_{eL} reversal, even though the density outside the V_{eL} reversal region increases from $4n_0$ at $y = 28.05d_i$ to $6n_0$ at $y = 26.05d_i$. The velocity V_{eN} is negative at the positive V_{eL} peak at $y = 27.2d_i$ in the simulation, while V_{eN} is positive when V_{eL} shows a positive peak in the observation. This difference is because the outflow jet in the simulation points in the upper right direction in panel (o), and the negative V_{eN} flow may be driven by the surrounding background flow. Also, as we explained, the positive electric field E_L in the outflow jet in the simulation is mainly due to the negative V_{eN} . Also, in the simulation, the magnitude of the reconnection electric field is comparable to the fluctuation amplitude of E_M and E_{\parallel} in the region surrounding the X line [panel (n)], while the observation [panel (g)] shows that the enhancement of the reconnection electric field is more pronounced than the simulation. This may be because $|B_M|$ (guide field) in the simulation is much smaller than in the observation, and the magnetic field direction in the simulation significantly fluctuates. This weaker guide field introduces larger-amplitude fluctuations in E_{\parallel} due to all the three components of the electric field, while the magnetic field in the observation always points almost in the negative M direction and the contribution of E_M , which has smaller fluctuations than E_L and E_N , dominates in E_{\parallel} .

In the simulation, the observed maximum outflow speed $(V_{eL}^2 + V_{eN}^2)^{1/2}$ along the black straight line is $12.3 v_{A0}$ at $y = 27.2d_i$, which is smaller than the actual maximum outflow speed in the simulation frame $15.4v_{A0}$ at $(x, y) = (48.525d_i, 27.35d_i)$. In addition, the maximum outflow speed in the X-line rest frame is $18v_{A0}$ (not shown). Therefore, this maximum outflow speed $12.3 v_{A0}$ on the black straight line is much smaller than the actual outflow speed V_{out} discussed in Sec. III B. As this example shows, the spacecraft data of the maximum outflow speed [panel (c)], 580 km/s ~ 22 times the Alfvén speed (or 440 km/s ~ 16 times the Alfvén speed, which is the difference between the outflow 580 km/s and the background flow 140 km/s), may be much smaller than the actual outflow speed in this reconnection region, and it is possible that the actual outflow speed is close to the electron Alfvén speed. Actually, other spacecraft in this event (in particular, MMS 3 and MMS 4, data not shown) observed faster outflow speeds by subtracting the background flow.

The observed outflow speed by MMS 1 ~ 16 – 22 times the Alfvén speed indicates that electron-only reconnection can generate a strong electron outflow of the order of the electron Alfvén speed, and a large reconnection electric field of the order of $RV_{out}B_d$ (in SI unit) is expected, where R is the reconnection rate. In this event, MMS observed an enhancement of electric field E_M up to around 4 mV/m near the B_L reversal point, which is much larger than an estimate using a standard reconnection picture, $E_M \sim 0.1B_d v_A \sim 0.014$ mV/m ($B_d = 5$ nT and $v_A = 27$ km/s). If we use an estimate of the reconnection rate in electron-only reconnection, $RB_d V_{out}$, we have $E_M \sim RB_d V_{out} \sim 0.7$ mV/m, using $R \sim 0.3$ and $V_{out} = 440$ km/s in the ion rest frame. The observed E_M , 4 mV/m, is much larger than this

estimate, indicating that either R is much larger than 0.3, or the actual maximum outflow speed V_{out} and the actual magnetic field at the edge of the EDR B_d are much larger than 440 km/s and 5 nT, respectively. For example, if $R = 0.5$ and $V_{out} \sim v_{Ae} \sim 1200$ km/s, E_M is estimated to be 3 mV/m. The observation clearly shows that the reconnection electric field is consistent with the prediction in this study.

V. CONCLUSIONS

In this paper, we have investigated magnetic reconnection in the shock transition region in a quasi-parallel shock, under parameters of the Earth's bow shock, by means of 2D PIC simulation. The shock normal angle is 25° , and the Alfvén Mach number is 11.4. We have analyzed the reconnection electric field, the reconnection rate, and the electron and ion outflow speeds in each reconnection site. From 43 X lines in the shock transition region observed in the simulation at $\Omega_i t = 18.75$, we have chosen 32 X lines that are stable for the analysis time interval for 100 time steps, and we have identified 18 electron-only reconnection sites and seven regular reconnection sites. In each reconnection site, we have measured the X-line velocity, and we have discussed quantities in the X-line stationary frame.

We have performed a statistical analysis for electron-only reconnection, to understand the relations between the reconnection electric field, the reconnection rate, and the electron outflow speed. The electron outflow speed and the theoretical prediction of the speed show a positive correlation, and electron-only reconnection can be understood using asymmetric reconnection theory by Ref. 20 by replacing the ion mass with the electron mass. We also have found a tendency that the reconnection electric field increases with the electron outflow speed, as well as the convection electric field due to the electron outflow. The reconnection rate is not a constant value such as 0.1, but it becomes larger when the product $V_{out}B_d/c$ becomes smaller. Also, the reconnection rate decreases with the increase in the guide field B_g , when B_g is larger than a few B_d (reconnecting magnetic field).

Regular reconnection in shock turbulence shows similar tendencies to those in electron-only reconnection. Both the electron outflow speed and the ion outflow speed become the order of $10 v_{A0}$, which is the same order as the upstream ion speed in the shock with $M_A = 11.4$. Although the electron outflow speed is not correlated with the theoretical speed, we have found a tendency that the electron outflow speed is proportional to the ion outflow speed. The reconnection electric field, as well as the reconnection rate, becomes the same order as that in electron-only reconnection, and the reconnection electric field increases with the increase in the convection electric field due to the electron outflow. The reconnection electric field and the reconnection rate show slight decreases when the guide field becomes larger than $3B_d$.

The magnitude of the reconnection electric field, both in electron-only reconnection and in regular reconnection, is unusually large, of the order of $0.1B_d V_{out}/c$. In electron-only reconnection, the reconnection electric field becomes $(m_i/m_e)^{1/2}$ times larger than that in reconnection in the Earth's magnetopause/magnetotail. This is understood as a result of the fast speed of electron outflow, of the order of local electron Alfvén speed, and the large convection electric field by the fast electron outflow. Surprisingly, the reconnection electric field in regular reconnection in the shock transition region also becomes the same order as that in electron-only reconnection, and

this is related to the large ion outflow and electron outflow, which also become much larger than Alfvén speed.

Reconnection in the shock is driven by instabilities: the nonresonant ion–ion instability and the secondary instability due to beams.¹⁴ The nonresonant ion–ion beam instability is caused by the ion reflection in the shock, and the reflected ion beam speed v_b is roughly proportional to the shock speed, $M_A v_{A0}$. The growth rate of the instability³⁴ is $\gamma/\Omega_i \sim v_b/v_{A0} = M_A$, which is a constant and does not depend on the upstream magnetic field B_0 and the mass ratio. Also, the growth rate is positive when the propagation angle is less than 45° , suggesting that the instability grows in a quasi-parallel shock. In contrast, the secondary instability is consistent with whistler waves excited by electron beams,¹⁴ and the growth rate is a function of B_0 and the mass ratio, whose leading order is $\gamma/\Omega_i \sim (n_b/n_0)(m_i/m_e)$.³⁵ Therefore, the growth rate normalized by Ω_i becomes larger as the mass ratio becomes larger. In a real shock ($m_i/m_e = 1840$), the growth of the secondary instability could be larger than that in the simulation in this study with $m_i/m_e = 200$. However, the above discussions are based on simplified linear analyses, and PIC simulations remain to be conducted to see the dependence of the instabilities and reconnection on B_0 , the shock angle, and the mass ratio.

An event of electron-only reconnection in the Earth’s magnetosheath downstream of a quasi-parallel shock, observed by MMS spacecraft, exhibits consistency with PIC simulation predictions. In the observed event, bipolar electron jets have been detected with a peak speed almost half the electron Alfvén speed. The outflow velocity reverses at around the magnetic field reversal point, indicating that the jets are generated near the reconnection X line. The event also shows the reconnection electric field that is much larger than the prediction based on the standard laminar reconnection, and closer to the prediction discussed in this paper, $E_M \sim RB_d v_{Ae}$. Further observational studies of electric fields in more events will help to better constrain the properties of reconnection electric fields and reconnection rates in both electron-only reconnection and regular reconnection in the Earth’s bow shock and the magnetosheath.

SUPPLEMENTARY MATERIAL

See the [supplementary material](#) for flow patterns, flow profiles, the size of the EDR, and the in-plane electric fields in a few reconnection sites.

ACKNOWLEDGMENTS

The work was supported by NASA Grant No. 80NSSC20K1312, DOE Grant No. DESC0016278, the NASA MMS project, and the Royal Society University Research Fellowship No. URF\R1\201286. PIC simulations were performed on Pleiades at the NASA Advanced Supercomputing, and the simulation data are available upon request from the authors.

AUTHOR DECLARATIONS

Conflict of Interest

The authors have no conflict of interest to disclose.

DATA AVAILABILITY

The data that support the findings of this study are available from the corresponding author upon reasonable request.

APPENDIX: OUTFLOW SPEED WITH THE L-DIRECTIONAL FLUXES

To argue V_{out} more precisely in a case where there are the L -directional mass and energy fluxes, let us obtain V_{out} as a function of v_{in-L} and n_{in-L}/n_{out} from Eq. (7). In that case, V_{out} is a solution of the following cubic equation:

$$V_{out}^3 - V_{theory}^2 V_{out} = \frac{n_{in-L}}{n_{out}} v_{in-L} (v_{in-L}^2 - V_{theory}^2). \tag{A1}$$

Let us investigate a solution of V_{out} as a function of v_{in-L} using a fixed value of n_{in-L}/n_{out} . The left-hand side is a cubic function of V_{out} , and let us denote it $f(V_{out})$. This function becomes zero at $V_{out} = 0$ and $V_{out} = V_{theory}$; that is, $f(0) = 0$ and $f(V_{theory}) = 0$. In $0 < V_{out} < V_{theory}$, $f(V_{out})$ takes its minimum value $-(2/3)(1/3)^{1/2} V_{theory}^3$ when $V_{out} = (1/3)^{1/2} V_{theory}$. Let us obtain the solution of V_{out} from $f(V_{out}) = a$, where a represents a value in the right-hand side of Eq. (A1), considering a crossing point of the curve $y = f(V_{out})$ and $y = a$. When v_{in-L} is zero, $a = 0$ and there are two solutions: One is $V_{out} = 0$, and the other is $V_{out} = V_{theory}$. In the following, we only consider the solution close to V_{theory} . We change v_{in-L} from zero to V_{theory} . As v_{in-L} increases, a becomes a negative value, and the solution of V_{out} becomes slightly smaller than V_{theory} . When $n_{in-L}/n_{out} < 1$, the range of a is $-(2/3)(1/3)^{1/2} V_{theory}^3 < a < 0$, and in this case, the solution of V_{out} is larger than $(1/3)^{1/2} V_{theory}$. When $n_{in-L}/n_{out} = 1$, the minimum value of a becomes $-(2/3)(1/3)^{1/2} V_{theory}^3$, and in that case, V_{out} takes its minimum value $(1/3)^{1/2} V_{theory} \sim 0.58 V_{theory}$. Therefore, the electron outflow speed V_{out} is not less than $0.58 V_{theory}$ under any values of n_{in-L}/n_{out} between zero and unity, and V_{out} is always of the order of V_{theory} .

Note that according to Eq. (A1), $V_{out} = V_{theory}$ when $v_{in-L} = V_{theory}$. When the ratio $n_{in-L}/n_{out} < 1$, this is understandable, because the sum of the three inflow fluxes related to v_{in1} , v_{in2} , and v_{in-L} is merged together to make a large outflow flux. However, when $n_{in-L} = n_{out}$, the condition that $V_{out} = V_{theory}$ and $v_{in-L} = V_{theory}$ means that there is no inflows of v_{in1} and v_{in2} , and this simply means that the L -directional inflow $v_{in-L} = V_{theory}$ is passing through the X line and the same speed of outflow V_{out} is realized in the outflow side. This is not reconnection. To realize reconnection, we require either $n_{in-L} < n_{out}$ or $V_{in-L} < V_{out}$. To see this point, let us see the inflow speed v_{in1} in Eqs. (3), (5), and (6). From these equations, we have the following relations:

$$\left(\frac{lv_{in1}}{2B_2\delta}\right)(n_1B_2 + n_2B_1) = n_{out}V_{out} - n_{in-L}v_{in-L}, \tag{A2}$$

$$\left(\frac{lv_{in1}}{2B_2\delta}\right)\frac{(B_1 + B_2)B_1B_2}{4\pi m_e} = n_{out}V_{out}^3 - n_{in-L}v_{in-L}^3. \tag{A3}$$

Looking into these equations, we find that v_{in1} becomes zero when $n_{in-L} = n_{out}$ and $V_{out} = v_{in-L}$. This is because the flux is coming in from the inflow direction with v_{in-L} and the same amount of flux is going out to the outflow direction with V_{out} . To make the inflow v_{in1} nonzero, we need to have either $n_{in-L} < n_{out}$ or $v_{in-L} < V_{out}$, and reconnection can occur only when one of the conditions is satisfied.

REFERENCES

- ¹T. D. Phan, J. P. Eastwood, M. A. Shay, J. F. Drake, B. U. Sonnerup, M. Fujimoto, P. A. Cassak, M. Øieroset, J. L. Burch, R. B. Torbert, A. C. Rager, J. C. Dorelli, D. J. Gershman, C. Pollock, P. S. Pyakurel, C. C. Haggerty, Y. Khotyaintsev, B. Lavraud, Y. Saito, M. Oka, R. E. Ergun, A. Retino, O. L. Contel, M. R. Argall, B. L. Giles, T. E. Moore, F. D. Wilder, R. J. Strangeway, C. T. Russell, P. A. Lindqvist, and W. Magnes, "Electron magnetic reconnection without ion coupling in Earth's turbulent magnetosheath," *Nature* **557**, 202 (2018).
- ²S. Wang, L.-J. Chen, N. Bessho, M. Hesse, L. B. Wilson, I. I. B. Giles, T. E. Moore, C. T. Russell, R. B. Torbert, and J. L. Burch, "Observational evidence of magnetic reconnection in the terrestrial bow shock transition region," *Geophys. Res. Lett.* **46**, 562, <https://doi.org/10.1029/2018GL080944> (2019).
- ³I. Gingell, S. J. Schwartz, J. P. Eastwood, J. L. Burch, R. E. Ergun, S. Fuselier, D. J. Gershman, B. L. Giles, Y. V. Khotyaintsev, B. Lavraud, P. A. Lindqvist, W. R. Paterson, T. D. Phan, C. T. Russell, J. E. Stawarz, R. J. Strangeway, R. B. Torbert, and F. Wilder, "Observations of magnetic reconnection in the transition region of quasi-parallel shocks," *Geophys. Res. Lett.* **46**, 1177 (2019).
- ⁴Z. Z. Chen, H. S. Fu, Z. Wang, C. M. Liu, and Y. Xu, "Evidence of magnetic nulls in the reconnection at bow shock," *Geophys. Res. Lett.* **46**, 10209, <https://doi.org/10.1029/2019GL084360> (2019).
- ⁵I. Gingell, S. J. Schwartz, J. P. Eastwood, J. E. Stawarz, J. L. Burch, R. E. Ergun, S. A. Fuselier, D. J. Gershman, B. L. Giles, Y. V. Khotyaintsev, B. Lavraud, P.-A. Lindqvist, W. R. Paterson, T. D. Phan, C. T. Russell, R. J. Strangeway, R. B. Torbert, and F. Wilder, "Statistics of reconnecting current sheets in the transition region of earth's bow shock," *J. Geophys. Res.* **125**, e2019JA027119, <https://doi.org/10.1029/2019JA027119> (2020).
- ⁶I. Gingell, S. J. Schwartz, H. Kucharek, C. J. Farrugia, and K. J. Trattner, "Observing the prevalence of thin current sheets downstream of Earth's bow shock," *Phys. Plasmas* **28**, 102902 (2021).
- ⁷J. E. Stawarz, J. P. Eastwood, T. D. Phan, I. L. Gingell, P. S. Pyakurel, M. A. Shay, S. L. Robertson, C. T. Russell, and L. Contel, "Turbulence-driven magnetic reconnection and the magnetic correlation length: Observations from magnetospheric multiscale in earth's magnetosheath," *Phys. Plasmas* **29**, 012302 (2022).
- ⁸S. Wang, L.-J. Chen, N. Bessho, M. Hesse, L. B. Wilson III, R. Denton, J. Ng, B. Giles, R. Torbert, and J. Burch, "Ion-scale current structures in short large-amplitude magnetic structures," *Astrophys. J.* **898**, 121 (2020).
- ⁹T. Z. Liu, S. Lu, D. L. Turner, I. Gingell, V. Angelopoulos, H. Zhang, A. Artemyev, and J. L. Burch, "Magnetospheric multiscale (MMS) observations of magnetic reconnection in foreshock transients," *J. Geophys. Res.* **125**, e2020JA027822, <https://doi.org/10.1029/2020JA027822> (2020).
- ¹⁰S. Lu, R. Wang, Q. Lu, V. Angelopoulos, R. Nakamura, A. V. Artemyev, P. L. Pritchett, T. Z. Liu, X.-J. Zhang, W. Baumjohann, W. Gonzalez, A. C. Rager, R. B. Torbert, B. L. Giles, D. J. Gershman, C. T. Russell, R. J. Strangeway, Y. Qi, R. E. Ergun, P.-A. Lindqvist, J. L. Burch, and S. Wang, "Magnetotail reconnection onset caused by electron kinetics with a strong external driver," *Nat. Commun.* **11**, 5049 (2020).
- ¹¹J. E. Stawarz, J. P. Eastwood, T. D. Phan, I. L. Gingell, M. A. Shay, J. L. Burch, R. E. Ergun, B. L. Giles, D. J. Gershman, L. Contel, P.-A. Lindqvist, C. T. Russell, R. J. Strangeway, R. B. Torbert, M. R. Argall, D. Fischer, W. Magnes, and L. Franc, "Properties of the turbulence associated with electron-only magnetic reconnection in earth's magnetosheath," *Astrophys. J. Lett.* **877**, L37 (2019).
- ¹²P. S. Pyakurel, M. A. Shay, T. D. Phan, W. H. Matthaeus, J. F. Drake, J. M. TenBarge, C. C. Haggerty, K. G. Klein, P. A. Cassak, T. N. Parashar, M. Swisdak, and A. Chasapis, "Transition from ion-coupled to electron-only reconnection: Basic physics and implications for plasma turbulence," *Phys. Plasmas* **26**, 082307 (2019).
- ¹³N. Bessho, L.-J. Chen, S. Wang, M. Hesse, and L. B. Wilson III, "Magnetic reconnection in a quasi-parallel shock: Two-dimensional local particle-in-cell simulation," *Geophys. Res. Lett.* **46**, 9352, <https://doi.org/10.1029/2019GL083397> (2019).
- ¹⁴N. Bessho, L.-J. Chen, S. Wang, M. Hesse, L. B. Wilson III, and J. Ng, "Magnetic reconnection and kinetic waves generated in the Earth's quasi-parallel bow shock," *Phys. Plasmas* **27**, 092901 (2020).
- ¹⁵C. Vega, V. Roytershteyn, G. L. Delzanno, and S. Boldyrev, "Electron-only reconnection in kinetic-Alfvén turbulence," *Astrophys. J. Lett.* **893**, L10 (2020).
- ¹⁶P. S. Pyakurel, M. A. Shay, J. F. Drake, T. D. Phan, P. A. Cassak, and J. L. Verniero, "Faster form of electron magnetic reconnection with a finite length X-line," *Phys. Rev. Lett.* **127**, 155101 (2021).
- ¹⁷G. Arró, F. Califano, and G. Lapenta, "Statistical properties of turbulent fluctuations associated with electron-only magnetic reconnection," *Astron. Astrophys.* **642**, A45 (2020).
- ¹⁸F. Califano, S. S. Cerri, M. Faganello, D. Laveder, M. Sisti, and M. W. Kunz, "Electron-only reconnection in plasma turbulence," *Front. Phys.* **8**, 317 (2020).
- ¹⁹T. K. M. Nakamura, S. Eriksson, H. Hasegawa, S. Zenitani, W. Y. Li, K. J. Genestreti, R. Nakamura, and W. Daughton, "Mass and energy transfer across the earth's magnetopause caused by vortex-induced reconnection," *J. Geophys. Res.* **122**, 11505, <https://doi.org/10.1002/2017JA024346> (2017).
- ²⁰P. A. Cassak and M. A. Shay, "Scaling of asymmetric magnetic reconnection: General theory and collisional simulations," *Phys. Plasmas* **14**, 102114 (2007).
- ²¹Y.-H. Liu, M. Hesse, F. Guo, H. Li, and T. K. M. Nakamura, "Strongly localized magnetic reconnection by the super-Alfvénic shear flow," *Phys. Plasmas* **25**, 080701 (2018).
- ²²J. Birn, J. F. Drake, M. A. Shay, B. N. Rogers, R. E. Denton, M. Hesse, M. Kuznetsova, Z. W. Ma, A. Bhattacharjee, A. Otto, and P. L. Pritchett, *Geophys. Res. Lett.* **106**, 3715, <https://doi.org/10.1029/1999JA900449> (2001).
- ²³P. A. Cassak, Y.-H. Liu, and M. A. Shay, "A review of the 0.1 reconnection rate problem," *J. Plasma Phys.* **83**, 715830501, <https://doi.org/10.1017/S0022377817000666> (2017).
- ²⁴R. B. Torbert, J. L. Burch, T. D. Phan, M. Hesse, M. R. Argall, J. Shuster, R. E. Ergun, L. Alm, R. Nakamura, K. J. Genestreti, D. J. Gershman, W. R. Paterson, D. L. Turner, I. Cohen, B. L. Giles, C. J. Pollock, S. Wang, L.-J. Chen, J. E. Stawarz, J. P. Eastwood, K. J. Hwang, C. Farrugia, I. Dors, H. Vaith, C. Moukiki, A. Ardakani, B. H. Mauk, S. A. Fuselier, C. T. Russell, R. J. Strangeway, T. E. Moore, J. F. Drake, M. A. Shay, Y. Khotyaintsev, P.-A. Lindqvist, W. Baumjohann, F. D. Wilder, N. Ahmadi, J. C. Dorelli, L. A. Avanov, M. Oka, D. N. Baker, J. F. Fennell, J. B. Blake, A. N. Jaynes, O. Le Contel, S. M. Petrinec, B. Lavraud, and Y. Saito, "Electron-scale dynamics of the diffusion region during symmetric magnetic reconnection in space," *Science* **362**, 1391 (2018).
- ²⁵J. L. Burch, J. M. Webster, M. Hesse, K. J. Genestreti, R. E. Denton, T. D. Phan, H. Hasegawa, P. A. Cassak, R. B. Torbert, B. L. Giles, D. J. Gershman, R. E. Ergun, C. T. Russell, R. J. Strangeway, O. Le Contel, K. R. Pritchard, A. T. Marshall, K.-J. Hwang, K. Dokgo, S. A. Fuselier, L.-J. Chen, S. Wang, M. Swisdak, J. F. Drake, M. R. Argall, K. J. Trattner, M. Yamada, and G. Paschmann, "Electron inflow velocities and reconnection rates at earth's magnetopause and magnetosheath," *Geophys. Res. Lett.* **47**, e2020GL089082, <https://doi.org/10.1029/2020GL089082> (2020).
- ²⁶Y.-H. Liu, M. Hesse, F. Guo, W. Daughton, H. Li, P. A. Cassak, and M. A. Shay, "Why does steady-state magnetic reconnection have a maximum local rate of order 0.1?," *Phys. Rev. Lett.* **118**, 085101 (2017).
- ²⁷C. T. Russell, B. J. Anderson, W. Baumjohann, K. R. Bromund, D. Dearborn, D. Fischer, G. Le, H. K. Leinweber, D. Leneman, W. Magnes, J. D. Means, M. B. Moldwin, R. Nakamura, D. Pierce, F. Plaschke, K. M. Rowe, J. A. Slavin, R. J. Strangeway, R. Torbert, C. Hagen, I. Jernej, A. Valavanoglou, and I. Richter, "The magnetospheric multiscale magnetometers," *Space Sci. Rev.* **199**, 189, <https://doi.org/10.1007/s11214-014-0057-3> (2014).
- ²⁸R. E. Ergun, S. Tucker, J. Westfall, K. A. Goodrich, D. M. Malaspina, D. Summers, J. Wallace, M. Karlsson, J. Mack, N. Brennan, B. Pyke, P. Withnell, R. Torbert, J. Macri, D. Rau, I. Dors, J. Needell, P.-A. Lindqvist, G. Olsson, and C. M. Cully, "The axial double probe and fields signal processing for the MMS mission," *Space Sci. Rev.* **199**, 167, <https://doi.org/10.1007/s11214-014-0115-x> (2014).
- ²⁹P.-A. Lindqvist, G. Olsson, R. B. Torbert, B. King, M. Granoff, D. Rau, G. Needell, S. Turco, I. Dors, P. Beckman, J. Macri, C. Frost, J. Salwen, A. Eriksson, L. Åhlén, Y. V. Khotyaintsev, J. Porter, K. Lappalainen, R. E. Ergun, W. Wimmer, and S. Tucker, "The spin-plane double probe electric field instrument for MMS," *Space Sci. Rev.* **199**, 137, <https://doi.org/10.1007/s11214-014-0116-9> (2014).

- ³⁰R. B. Torbert, C. T. Russell, W. Magnes, R. E. Ergun, P.-A. Lindqvist, O. LeContel, H. Vaith, J. Macri, S. Myers, D. Rau, J. Needell, B. King, M. Granoff, M. Chutter, I. Dors, G. Olsson, Y. V. Khotyaintsev, A. Eriksson, C. A. Kletzing, S. Bounds, B. Anderson, W. Baumjohann, M. Steller, K. Bromund, G. Le, R. Nakamura, R. J. Strangeway, H. K. Leinweber, S. Tucker, J. Westfall, D. Fischer, F. Plaschke, J. Porter, and K. Lappalainen, “The FIELDS instrument suite on MMS: Scientific objectives, measurements, and data products,” *Space Sci. Rev.* **199**, 105, <https://doi.org/10.1007/s11214-014-0109-8> (2014).
- ³¹C. Pollock, T. Moore, A. Jacques, J. Burch, U. Gliese, Y. Saito, T. Omoto, L. Avanov, A. Barrie, V. Coffey, J. Dorelli, D. Gershman, B. Giles, T. Rosnack, C. Salo, S. Yokota, M. Adrian, C. Aoustin, C. Auletta, S. Aung, V. Bigio, N. Cao, M. Chandler, D. Chornay, K. Christian, G. Clark, G. Collinson, T. Corris, A. de Los Santos, R. Devlin, T. Diaz, T. Dickerson, C. Dickson, A. Diekmann, F. Diggs, C. Duncan, A. Figueroa-Vinas, C. Firman, M. Freeman, N. Galassi, K. Garcia, G. Goodhart, D. Guerro, J. Hageman, J. Hanley, E. Hemminger, M. Holland, M. Hutchins, T. James, W. Jones, S. Kreisler, J. Kujawski, V. Lavu, J. Lobell, E. LeCompte, A. Lukemire, E. MacDonald, A. Mariano, T. Mukai, K. Narayanan, Q. Nguyen, M. Onizuka, W. Paterson, S. Persyn, B. Piepgrass, F. Cheney, A. Rager, T. Raghuram, A. Ramil, L. Reichenthal, H. Rodriguez, J. Rouzau, A. Rucker, Y. Saito, M. Samara, J. A. Sauvaud, D. Schuster, M. Shappirio, K. Shelton, D. Sher, D. Smith, K. Smith, S. Smith, D. Steinfeld, R. Szymkiewicz, K. Tanimoto, J. Taylor, C. Tucker, K. Tull, A. Uhl, J. Vloet, P. Walpole, S. Weidner, D. White, G. Winkert, P. S. Yeh, and M. Zeuch, “Fast plasma investigation for magnetospheric multiscale,” *Space Sci. Rev.* **199**, 331–406, <https://doi.org/10.1007/s11214-016-0245-4> (2016).
- ³²J. T. Gosling and T. D. Phan, “Magnetic reconnection in the solar wind at current sheets associated with extremely small field shear angles,” *Astrophys. J. Lett.* **763**, L39 (2013).
- ³³F. D. Wilder, R. E. Ergun, S. Eriksson, T. D. Phan, J. L. Burch, N. Ahmadi, K. A. Goodrich, D. L. Newman, K. J. Trattner, R. B. Torbert, B. L. Giles, R. J. Strangeway, W. Magnes, P.-A. Lindqvist, and Y.-V. Khotyaintsev, “Multipoint measurements of the electron jet of symmetric magnetic reconnection with a moderate guide field,” *Phys. Rev. Lett.* **118**, 265101 (2017).
- ³⁴S. P. Gary, “Electromagnetic ion/ion instabilities and their consequences in space plasmas: A review,” *Space Sci. Rev.* **56**, 373, <https://doi.org/10.1007/BF00196632> (1991).
- ³⁵H. K. Wong and C. W. Smith, “Electron beam excitation of upstream waves in the whistler mode frequency range,” *J. Geophys. Res.* **99**, 13373, <https://doi.org/10.1029/94JA00821> (1994).